Elastic modeling of point-defects and their interaction

Emmanuel Clouet, Céline Varvenne, Thomas Jourdan

Elastic modeling of point-defects and their interaction

Emmanuel Clouet[a,*], Céline Varvenne[b], Thomas Jourdan[a]

[a] *DEN-Service de Recherches de Métallurgie Physique, CEA,Paris-Saclay Univ., F-91191 Gif-sur-Yvette, France*
[b] *Centre Interdisciplinaire des Nanosciences de Marseille, UMR 7325 CNRS - Aix Marseille Univ., F-13008 Marseille, France*

Abstract

Different descriptions used to model a point-defect in an elastic continuum are reviewed. The emphasis is put on the elastic dipole approximation, which is shown to be equivalent to the infinitesimal Eshelby inclusion and to the infinitesimal dislocation loop. Knowing this elastic dipole, a second rank tensor fully characterizing the point-defect, one can directly obtain the long-range elastic field induced by the point-defect and its interaction with other elastic fields. The polarizability of the point-defect, resulting from the elastic dipole dependence with the applied strain, is also introduced. Parameterization of such an elastic model, either from experiments or from atomic simulations, is discussed. Different examples, like elastodiffusion and bias calculations, are finally considered to illustrate the usefulness of such an elastic model to describe the evolution of a point-defect in a external elastic field.

Keywords: Point-defects, Elasticity, Elastic dipole, Polarizability

1. Introduction

Point-defects in crystalline solids, being either intrinsic like vacancies, self-interstitial atoms, and their small clusters, or extrinsic like impurities and dopants, play a major role in materials properties and their kinetic evolution. Some properties of these point-defects, like their formation and migration energies, are mainly determined by the region in the immediate vicinity of the defect where the crystal structure is strongly perturbed. An atomic description appears thus natural to model these properties, and atomic simulations relying either on *ab initio* calculations [1] or empirical potentials have now become a routine tool to study point-defects structures and energies. But point-defects also induce a long-range perturbation of the host lattice, leading to an elastic interaction with other structural defects, impurities or an applied elastic field. An atomic description thus appears unnecessary to capture the interaction arising from this long-range part, and sometimes is also impossible because of the reduced size of the simulation cell in atomic approaches. Elasticity theory becomes then the natural framework. It allows a quantitative description of the point-defect interaction with other defects.

Following the seminal work of Eshelby [2], the simplest elastic model of a point-defect corresponds to a spherical inclusion forced into a spherical hole of slightly different size in an infinite elastic medium. This description accounts for the point-defect relaxation volume and its interaction with a pressure field (size interaction). It can be enriched by considering an ellipsoidal inclusion, thus leading to a interaction with also the deviatoric component of the stress field (shape interaction), and by assigning different elastic constants to the inclusion (inhomogeneity) to describe the variations of the point-defect "size" and "shape" with the strain field where it is immersed. Other elastic descriptions of the point-defect are possible. In particular, it can be modeled by an equivalent distribution of point-forces. The long-range elastic field of the point-defect and its interaction with other stress sources are then fully characterized by the first moment of this force distribution, a second-rank tensor called the elastic dipole. This description is rather natural when modeling point-defects and it can be used

*Corresponding author
Email address: emmanuel.clouet@cea.fr (Emmanuel Clouet)

to extract elastic dipoles from atomic simulations. These different descriptions are equivalent in the long-range limit, and allow for a quantitative modeling of the elastic field induced by the point-defect, as long as the elastic anisotropy of the matrix is considered.

This article reviews these different elastic models which can be used to describe a point-defect and illustrates their usefulness with chosen examples. After a short reminder of elasticity theory (Sec. 2), we introduce the different descriptions of a point-defect within elasticity theory (Sec. 3), favoring the elastic dipole description and showing its equivalence with the infinitesimal Eshelby inclusion as well as with an infinitesimal dislocation loop. The next section (Sec. 4) describes how the characteristics of the point-defect needed to model it within elasticity theory can be obtained either from atomistic simulations or from experiments. We finally give some applications in Sec. 5, where results of such an elastic model are compared to direct atomic simulations to assess its validity. The usefulness of this elastic description is illustrated in this section for elastodiffusion and for the calculation of bias factors, as well as for the modeling of isolated point-defects in atomistic simulations.

2. Elasticity theory

Before describing the modeling of a point-defect within elasticity theory, it is worth recalling the main aspects of the theory [3], in particular the underlying assumptions, some definitions and useful results.

2.1. Displacement, distortion and strain

Elasticity theory is based on a continuous description of solid bodies. It relates the forces, either internal or external, exerting on the solid to its deformation. To do so, one first defines the elastic displacement field. If $\vec{R}$ and $\vec{r}$ are the position of a point respectively in the unstrained and the strained body, the displacement at this point is given by

$$\vec{u}(\vec{R}) = \vec{r} - \vec{R}.$$

One can then define the distortion tensor $\partial u_i \,/\, \partial R_j$ which expresses how an infinitesimal vector $\overrightarrow{\mathrm{d}R}$ in the unstrained solid is transformed in $\overrightarrow{\mathrm{d}r}$ in the strained body through the relation

$$\mathrm{d}r_i = \left(\delta_{ij} + \frac{\partial u_i}{\partial R_j}\right) \mathrm{d}R_j,$$

where summation over repeated indices is implicit (Einstein convention) and δ_{ij} is the Kronecker symbol.

Of central importance to the elasticity theory is the dimensionless strain tensor, defined by

$$\begin{aligned}\varepsilon_{ij}(\vec{R}) &= \frac{1}{2}\left[\left(\delta_{in} + \frac{\partial u_n}{\partial R_i}\right)\left(\delta_{nj} + \frac{\partial u_n}{\partial R_j}\right) - \delta_{ij}\right] \\ &= \frac{1}{2}\left(\frac{\partial u_i}{\partial R_j} + \frac{\partial u_j}{\partial R_i} + \frac{\partial u_n}{\partial R_i}\frac{\partial u_n}{\partial R_j}\right).\end{aligned}$$

This symmetric tensor expresses the change of size and shape of a body as a result of a force acting on it. The length $\mathrm{d}L$ of the infinitesimal vector $\overrightarrow{\mathrm{d}R}$ in the unstrained body is thus transformed into $\mathrm{d}l$ in the strained body, through the relation

$$\mathrm{d}l^2 = \mathrm{d}L^2 + 2\varepsilon_{ij}\mathrm{d}R_i\mathrm{d}R_j.$$

Assuming small deformation, a common assumption of linear elasticity, only the leading terms of the distortion are kept. The strain tensor then corresponds to the symmetric part of the distortion tensor, as

$$\varepsilon_{ij}(\vec{R}) = \frac{1}{2}\left(\frac{\partial u_i}{\partial R_j} + \frac{\partial u_j}{\partial R_i}\right). \tag{1}$$

The antisymmetric part of the distortion tensor corresponds to the infinitesimal rigid body rotation. It does not lead to any energetic contribution within linear elasticity in the absence of internal torque.

With this small deformation assumption, there is no distinction between Lagrangian coordinates $\vec{R}$ and Eulerian coordinates $\vec{r}$ when describing elastic fields. One can equally write, for instance, $\vec{u}(\vec{r})$ or $\vec{u}(\vec{R})$ for the displacement field, which are equivalent to the leading order of the distortion.

2.2. Stress

The force $\overrightarrow{\delta F}$ acting on a volume element δV of a strained body is composed of two contributions, the sum of external body forces $\vec{f}$ and the internal forces arising from atomic interactions. Because of the mutual cancellation of forces between particles inside the volume δV, only forces corresponding to the interaction with outside particles appear in this last contribution, which is thus proportional to the surface elements $\overrightarrow{\mathrm{d}S}$ defining the volume element δV. One obtains

$$\delta F_i = \int_{\delta V} f_i \mathrm{d}V + \oint_{\delta S} \sigma_{ij}\mathrm{d}S_j,$$

where σ is the stress tensor defining internal forces.

Considering the mechanical equilibrium of the volume element δV, the absence of resultant force leads to the equation

$$\frac{\partial \sigma_{ij}(\vec{r})}{\partial r_j} + f_i(\vec{r}) = 0, \tag{2}$$

whereas the absence of torque ensures the symmetry of the stress tensor.

At the boundary of the strained body, internal forces are balanced by applied forces. If $\vec{T}^{\mathrm{a}}\mathrm{d}S$ is the force applied on the infinitesimal surface element $\mathrm{d}S$, this leads to the boundary condition

$$\sigma_{ij} n_j = T_i^{\mathrm{a}}, \tag{3}$$

where $\vec{n}$ is the outward-pointing normal to the surface element $\mathrm{d}S$.

The work δw, defined per volume unit, of these internal forces is given by

$$\delta w = -\sigma_{ij} \delta \varepsilon_{ij},$$

where $\delta \varepsilon_{ij}$ is the strain change during the deformation increase, and the sign convention is $\delta w > 0$ when the energy flux goes outwards the elastic body. This leads to the following thermodynamic definition of the stress tensor

$$\sigma_{ij} = \left(\frac{\partial e}{\partial \varepsilon_{ij}} \right)_s = \left(\frac{\partial f}{\partial \varepsilon_{ij}} \right)_T,$$

where e, s, and $f = e - Ts$ are the internal energy, entropy, and free energy of the elastic body defined per volume unit.

2.3. Hooke's law

To go further, one needs a constitutive equation for the energy or the free energy. Taking as a reference the undeformed state corresponding to the elastic body at equilibrium without any external force, either body or applied stress, the energy is at a minimum for $\varepsilon = 0$ and then

$$\sigma_{ij}(\varepsilon = 0) = \left. \frac{\partial e}{\partial \varepsilon_{ij}} \right|_{\varepsilon = 0} = 0.$$

The leading order terms of the series expansion of the energy are then

$$e(T, \varepsilon) = e^0(T) + \frac{1}{2} C_{ijkl} \varepsilon_{ij} \varepsilon_{kl},$$

where $e^0(T) = e(T, \varepsilon = 0)$ is the energy of the unstrained body at temperature T. The elastic constants C_{ijkl} entering this expression are thus defined by

$$C_{ijkl} = \frac{\partial^2 e}{\partial \varepsilon_{ij} \partial \varepsilon_{kl}}.$$

This is a fourth-rank tensor which obeys minor symmetry $C_{ijkl} = C_{jikl} = C_{ijlk}$ because of the strain tensor symmetry and also major symmetry $C_{ijkl} = C_{klij}$ because of allowed permutation of partial derivatives. This leads to at most 21 independent coefficients, which can be further reduced by considering the symmetries of the solid body [4].

This series expansion of the energy leads to a linear relation, the Hooke's law, between the stress and the strain

$$\sigma_{ij} = C_{ijkl} \varepsilon_{kl}, \tag{4}$$

which was summarized in 1678 by Robert Hooke as *Ut tensio, sic vis.*[1]

2.4. Elastic equilibrium, superposition principle

Combining Hooke's law (4) with the small deformation definition (1) of the strain tensor and the equilibrium condition (2), one obtains the equation obeyed by the displacement at equilibrium

$$C_{ijkl} \frac{\partial^2 u_k(\vec{r})}{\partial r_j \partial r_l} + f_i(\vec{r}) = 0. \tag{5}$$

The elastic equilibrium is given by the solution which verifies the boundary conditions, $\sigma_{ij} n_j = T_i^{\mathrm{a}}$ for imposed applied forces and $u_i = u_i^{\mathrm{a}}$ for imposed applied displacements.

As elastic equilibrium is defined by the solution of a linear partial differential equation (Eq. 5), the superposition principle holds. If two elastic fields, characterized by their displacement $\vec{u}^1(\vec{r})$ and $\vec{u}^2(\vec{r})$, correspond to equilibrium for the respective body forces $\vec{f}^1$ and $\vec{f}^2$ and the respective boundary conditions $(\vec{u}^{\mathrm{a}1}, \vec{T}^{\mathrm{a}1})$ and $(\vec{u}^{\mathrm{a}2}, \vec{T}^{\mathrm{a}2})$, then the elastic equilibrium for the body forces $\vec{f}^1 + \vec{f}^2$ and the boundary conditions $(\vec{u}^{\mathrm{a}1} + \vec{u}^{\mathrm{a}2}, \vec{T}^{\mathrm{a}1} + \vec{T}^{\mathrm{a}2})$ is given by the sum of these two elastic fields. The total elastic energy is composed of the contributions of each elastic field taken separately and an

[1] As the extension, so the force.

interaction energy given by

$$\begin{aligned} E^{\text{int}} &= \int_V \sigma^1_{ij}(\vec{r})\,\varepsilon^2_{ij}(\vec{r})\,\mathrm{d}V \\ &= \int_V \sigma^2_{ij}(\vec{r})\,\varepsilon^1_{ij}(\vec{r})\,\mathrm{d}V. \end{aligned} \tag{6}$$

This equation can be used to define interaction energy between two defects.

The superposition principle allows making use of Green's function. The elastic Green's function $G_{kn}(\vec{r})$ is the solution of the equilibrium equation for a unit point-force

$$C_{ijkl}\frac{\partial^2 G_{kn}(\vec{r})}{\partial r_j \partial r_l} + \delta_{in}\,\delta(\vec{r}) = 0, \tag{7}$$

where $\delta(\vec{r})$ is the Dirac delta function, *i.e.* $\delta(\vec{r}) = 0$ if $\vec{r} \neq \vec{0}$ and $\delta(\vec{0}) = \infty$. $G_{kn}(\vec{r})$ therefore corresponds to the displacement along the r_k axis for a unit point-force applied along the r_n axis at the origin. The solution of elastic equilibrium for the force distribution $\vec{f}(\vec{r})$ is then given by

$$\begin{aligned} u_k(\vec{r}) &= \int_V G_{kn}(\vec{r}-\vec{r}\,')f_n(\vec{r}\,')\mathrm{d}V', \\ \sigma_{ij}(\vec{r}) &= C_{ijkl}\int_V G_{kn,l}(\vec{r}-\vec{r}\,')f_n(\vec{r}\,')\mathrm{d}V', \end{aligned}$$

where we have introduced the notation $G_{kn,l} = \partial G_{kn} \,/\, \partial r_l$ for partial derivatives.

An analytical expression of the Green's function exists for isotropic elasticity. Considering the elastic constants $C_{ijkl} = \lambda\delta_{ij}\delta_{kl} + \mu(\delta_{ik}\delta_{jl} + \delta_{il}\delta_{jk})$, where λ and μ are the Lamé coefficients, the Green's function is given by

$$G_{kn}(\vec{r}) = \frac{1}{8\pi\mu}\left[\frac{\lambda+3\mu}{\lambda+2\mu}\delta_{kn} + \frac{\lambda+\mu}{\lambda+2\mu}\eta_k\eta_n\right]\frac{1}{r},$$

with $r = \|\vec{r}\|$ and $\vec{\eta} = \vec{r}/r$. No analytical expression exists in the more general case of elastic anisotropy, but the Green's function, and its successive derivatives, can be calculated efficiently from the elastic constants using the numerical scheme of Barnett [5, 6]. Whatever the anisotropy, the Green's function and its derivatives will show the same variation with the distance r,[2] leading to the general expressions

$$G_{kn}(\vec{r}) = g_{kn}(\vec{\eta})\frac{1}{r}\ ,\ G_{kn,l}(\vec{r}) = h_{knl}(\vec{\eta})\frac{1}{r^2}\ ,\ \ldots$$

where the anisotropy enters only in the angular dependence $g_{kn}(\vec{\eta})$, $h_{knl}(\vec{\eta})$, ...

3. Elastic model of a point-defect

Different models can be used to describe a point-defect within elasticity theory. One such model is the elastic dipole. We first describe this model and then demonstrate the analogy with a description of the point-defect as an infinitesimal Eshelby inclusion or an infinitesimal dislocation loop. We finally introduce the polarizability of the point-defect.

3.1. Elastic dipole

A point-defect can be described in a continuous solid body as an equilibrated distribution of point-forces [6–9]. Considering a point-defect located at the origin modeled by such a force distribution $\vec{f}(\vec{r}) = \sum_{q=1}^{N}\vec{F}^q\,\delta\,(\vec{r}-\vec{a}^q)$, *i.e.* consisting of N forces $\vec{F}^q$ each acting at position $\vec{a}^q$, the elastic displacement field of the point-defect is, according to linear elasticity theory, given by

$$u_i(\vec{r}) = \sum_{q=1}^{N} G_{ij}(\vec{r}-\vec{a}^q)F^q_j,$$

where we have used the elastic Green's function. Far from the point-defect, we have $\|\vec{r}\| \gg \|\vec{a}^q\|$ and we can make a series expansion of the Green's function:

$$\begin{aligned} u_i(\vec{r}) = G_{ij}(\vec{r})\sum_{q=1}^{N}F^q_j \ -\ G_{ij,k}(\vec{r})\sum_{q=1}^{N}F^q_j a^q_k \\ +\ \mathrm{O}\left(\|\vec{a}^q\|^2\right). \end{aligned}$$

As the force distribution is equilibrated, its resultant $\sum_q \vec{F}^q$ is null. The displacement is thus given, to the leading order, by

$$u_i(\vec{r}) = -G_{ij,k}(\vec{r})P_{jk}, \tag{8}$$

and the corresponding stress field by

$$\sigma_{ij}(\vec{r}) = -C_{ijkl}G_{km,nl}(\vec{r})P_{mn}, \tag{9}$$

where the elastic dipole is defined as the first moment of the point-force distribution,

$$P_{jk} = \sum_{q=1}^{N} F^q_j a^q_k. \tag{10}$$

[2] The scaling with the distance r is a consequence of Eq. (7), given that the $\delta(\vec{r})$ function is homogeneous of degree -3.

This dipole is a second rank tensor which fully characterizes the point-defect within elasticity theory [6–9]. It is symmetric because the torque $\sum_q \vec{F}^q \times \vec{a}^q$ must be null for the force distribution to be equilibrated.

Equations (8) and (9) show that the elastic displacement and the stress created by a point-defect are long-ranged, respectively decaying as $1/r^2$ and $1/r^3$ with the distance r to the point-defect.

The elastic dipole is directly linked to the point-defect relaxation volume. Considering a finite volume V of external surface S enclosing the point-defect, this relaxation volume is defined as

$$\Delta V = \oint_S u_i(\vec{r})\, \mathrm{d}S_i,$$

where $\vec{u}(\vec{r})$ is the superposition of the displacement created by the point-defect (Eq. 8) and the elastic displacement due to image forces ensuring null tractions on the external surface S. Use of the Gauss theorem, of the equilibrium condition (5) and of the elastic dipole definition (10) leads to the result [8]

$$\Delta V = S_{iikl} P_{kl}, \tag{11}$$

where the elastic compliances S_{ijkl} are the inverse of the elastic constants, *i.e.* $S_{ijkl} C_{klmn} = \frac{1}{2}(\delta_{im}\delta_{jn} + \delta_{in}\delta_{jm})$. For a crystal with cubic symmetry, this equation can be further simplified [8] to show that the relaxation volume is equal to the trace of the elastic dipole divided by three times the bulk modulus. More generally, as it will become clear with the comparison to the Eshelby's inclusion, this elastic dipole is the source term defining the relaxation volume of the point-defect. Its trace gives rise to the size interaction, whereas its deviator, *i.e.* the presence of off-diagonal terms and differences in the diagonal components, leads to the shape interaction.

Of particular importance is the interaction energy of the point-defect with an external elastic field $\vec{u}^{\mathrm{ext}}(\vec{r})$. Considering the point-forces distribution representative of the point-defect, this interaction energy can be simply written as [6]

$$E^{\mathrm{int}} = -\sum_{q=1}^{N} F_i^q\, u_i^{\mathrm{ext}}(\vec{a}^q).$$

If we now assume that the external field is slowly varying close to the point-defect, one can make a series expansion of the corresponding displacement $\vec{u}^{\mathrm{ext}}(\vec{r})$. The interaction energy is then, to first order,

$$E^{\mathrm{int}} = -u_i^{\mathrm{ext}}(\vec{0}) \sum_{q=1}^{N} F_i^q - u_{i,j}^{\mathrm{ext}}(\vec{0}) \sum_{q=1}^{N} F_i^q\, a_j^q.$$

Finally, using the equilibrium properties of the point-forces distribution, one obtains

$$E^{\mathrm{int}} = -P_{ij}\, \varepsilon_{ij}^{\mathrm{ext}}(\vec{0}), \tag{12}$$

thus showing that the interaction energy is simply the product of the elastic dipole with the value at the point-defect location of the external strain field. Higher order contributions to the interaction energy involve successive gradients of the external strain field coupled with higher moments of the multipole expansion of the force distribution, and can be generally safely ignored. This simple expression of the interaction energy is the workhorse of the modeling of point-defects within linear elasticity in a multiscale approach.

Instead of working with the elastic dipole tensor, one sometimes rather uses the so-called λ-tensor [10] which expresses the strain variation of a matrix volume with the point-defect volume concentration c,

$$\lambda_{ij} = \frac{1}{\Omega_{\mathrm{at}}} \frac{\partial \bar{\varepsilon}_{ij}}{\partial c}, \tag{13}$$

where $\bar{\varepsilon}$ is the homogeneous strain induced by the point-defects in a stress-free state and Ω_{at} is the atomic volume of the reference solid. As it will become clear when discussing parameterization of the elastic dipole from experiments (§4.2), these two quantities are simply linked by the relation

$$P_{ij} = \Omega_{\mathrm{at}}\, C_{ijkl}\, \lambda_{kl}. \tag{14}$$

Using this λ-tensor to characterize the point-defect, Eq. (12) describing its elastic interaction with an external elastic field becomes

$$E^{\mathrm{int}} = -\Omega_{\mathrm{at}}\, \lambda_{ij}\, \sigma_{ij}^{\mathrm{ext}}(\vec{0}),$$

where $\sigma_{ij}^{\mathrm{ext}}(\vec{0})$ is the value of the external stress field at the point-defect position.

3.2. Analogy with Eshelby's inclusion

The Eshelby's inclusion [11, 12] is another widespread model which can be used to describe a point-defect in an elastic continuum. As it will be shown below, it is equivalent to the dipole description in the limit of an infinitesimal inclusion.

In this model, the point-defect is described as an inclusion of volume $\Omega_{\rm I}$ and of surface $S_{\rm I}$, having the same elastic constants as the matrix. This inclusion undergoes a change of shape described by the eigenstrain $\varepsilon^*_{ij}(\vec{r})$, corresponding to the strain that would adopt the inclusion if it was free to relax and was not constrained by the surrounding matrix. Eshelby proposed a general approach [11] to solve the corresponding equilibrium problem and determine the elastic fields in the inclusion and the surrounding matrix. This solution is obtained by considering the three following steps:

1. Take the inclusion out of the matrix and let it adopt its eigenstrain $\varepsilon^*_{ij}(\vec{r})$. At this stage, the stress is null everywhere.
2. Strain back the inclusion so it will fit the hole in the matrix. The elastic strain exactly compensates for the eigenstrain, so the stress in the inclusion is $-C_{ijkl}\varepsilon^*_{kl}(\vec{r})$. This operation is performed by applying to the external surface of the inclusion the traction forces corresponding to this stress
$$\mathrm{d}T_i(\vec{r}) = -C_{ijkl}\,\varepsilon^*_{kl}(\vec{r})\,\mathrm{d}S_j,$$
where $\overrightarrow{\mathrm{d}S}$ is an element of the inclusion external surface at the point $\vec{r}$.
3. After the inclusion has been welded back into its hole, the traction forces are relaxed. Using Green's function, the corresponding displacement in the matrix is then
$$\begin{aligned} u_n(\vec{r}) &= \oint_{S_{\rm I}} G_{ni}(\vec{r}-\vec{r}\,')\,\mathrm{d}T_i(\vec{r}\,'), \\ &= -\oint_{S_{\rm I}} G_{ni}(\vec{r}-\vec{r}\,')\,C_{ijkl}\,\varepsilon^*_{kl}(\vec{r}\,')\,\mathrm{d}S'_j. \end{aligned}$$

Applying Gauss theorem and the equilibrium condition satisfied by the eigenstrain $\varepsilon^*_{ij}(\vec{r})$, one obtains the following expression for the elastic displacement in the matrix

$$u_n(\vec{r}) = -\int_{\Omega_{\rm I}} G_{ni,j}(\vec{r}-\vec{r}\,')\,C_{ijkl}\,\varepsilon^*_{kl}(\vec{r}\,')\,\mathrm{d}V', \tag{15}$$

and for the corresponding stress field

$$\sigma_{pq}(\vec{r}) = -\int_{\Omega_{\rm I}} C_{pqmn}\,G_{ni,jm}(\vec{r}-\vec{r}\,')\,C_{ijkl}\,\varepsilon^*_{kl}(\vec{r}\,')\,\mathrm{d}V'. \tag{16}$$

Inside the inclusion, one needs to add the stress $-C_{ijkl}\varepsilon^*_{kl}(\vec{r})$ corresponding to the strain applied in step 2.

Far from the inclusion, we have $\|\vec{r}\| \gg \|\vec{r}\,'\|$. We can therefore neglect the variations of the Green's function derivatives inside Eqs. 15 and 16. This corresponds to the infinitesimal inclusion assumption. For such an infinitesimal inclusion located at the origin, one therefore obtains the following elastic fields

$$u_n(\vec{r}) = -G_{ni,j}(\vec{r})\,C_{ijkl}\,\Omega_{\rm I}\,\bar{\varepsilon}^*_{kl}, \tag{17}$$
$$\sigma_{pq}(\vec{r}) = -C_{pqmn}\,G_{ni,jm}(\vec{r})\,C_{ijkl}\,\Omega_{\rm I}\,\bar{\varepsilon}^*_{kl}, \tag{18}$$

where we have defined the volume average of the inclusion eigenstrain, $\bar{\varepsilon}^*_{ij} = \frac{1}{\Omega_{\rm I}}\int_{\Omega_{\rm I}} \varepsilon_{ij}(\vec{r})\,\mathrm{d}V$. Comparing these expressions with the ones describing the elastic field of an elastic dipole (Eqs. 8 and 9), we see that they are the same for any $\vec{r}$ value provided the dipole tensor and the inclusion eigenstrain check the relation

$$P_{ij} = \Omega_{\rm I}\,C_{ijkl}\,\bar{\varepsilon}^*_{kl}. \tag{19}$$

The descriptions of a point-defect as an elastic dipole, *i.e.* as a distribution of point-forces keeping only the first moment of the distribution, or as an infinitesimal Eshelby inclusion, *i.e.* in the limit of an inclusion volume $\Omega_{\rm I} \to 0$ keeping the product $\Omega_{\rm I}\,\bar{\varepsilon}^*_{ij}$ constant, are therefore equivalent. The point-defect can be thus characterized either by its elastic dipole tensor P_{ij} or by its eigenstrain tensor $Q_{ij} = \Omega_{\rm I}\,\bar{\varepsilon}^*_{ij}$ [13].

Of course, the same equivalence is obtained when considering the interaction energy with an external stress field. For a general inclusion, Eshelby showed that this interaction energy is simply given by

$$E^{\rm int} = -\int_{\Omega_{\rm I}} \varepsilon^*_{ij}(\vec{r})\,\sigma^{\rm ext}_{ij}(\vec{r})\,\mathrm{d}V, \tag{20}$$

where the integral only runs on the inclusion volume. In the limiting case of an infinitesimal inclusion, one can neglect the variations of the external stress field inside the inclusion. One thus obtains the following interaction energy,

$$E^{\rm int} = -\Omega_{\rm I}\,\bar{\varepsilon}^*_{ij}\,\sigma^{\rm ext}_{ij}(\vec{0}), \tag{21}$$

which is equivalent to the expression (12) for an elastic dipole when the equivalence relation (19) is verified.

3.3. Analogy with dislocation loops

A point-defect can also be considered as an infinitesimal dislocation loop. This appears natural as dislocation loops are known to be elastically equivalent to platelet Eshelby's inclusions [14, 15].

The elastic displacement and stress fields of a dislocation loop of Burgers vector $\vec{b}$ are respectively given by the Burger's and the Mura's formulae [16]

$$u_i(\vec{r}) = C_{jklm}\, b_m \int_A G_{ij,k}(\vec{r}-\vec{r}')\, n_l(\vec{r}')\, \mathrm{d}A', \tag{22}$$

$$\sigma_{ij}(\vec{r}) = C_{ijkl}\, \epsilon_{lnh} C_{pqmn} b_m \oint_L G_{kp,q}(\vec{r}-\vec{r}')\, \zeta_h(\vec{r}')\, \mathrm{d}l'. \tag{23}$$

The displacement is defined by a surface integral on the surface A enclosed by the dislocation loop, with $\vec{n}(\vec{r}')$ the local normal to the surface element $\mathrm{d}A'$ in $\vec{r}'$, and the stress by a line integral along the loop of total line length L. $\vec{\zeta}$ is the unit vector along the loop, and ϵ_{lnh} is the permutation tensor.

Like for the Eshelby's inclusion, far from the loop ($\|\vec{r}\| \gg \|\vec{r}'\|$), we can use a series expansion of the Green's function derivatives and keep only the leading term. Considering a loop located at the origin, we thus obtain

$$u_i(\vec{r}) = C_{jklm}\, b_m\, A_l\, G_{ij,k}(\vec{r}), \tag{24}$$

$$\sigma_{pq}(\vec{r}) = C_{pqin}\, C_{jklm}\, b_m\, A_l\, G_{ij,kn}(\vec{r}), \tag{25}$$

where $\vec{A}$ is the surface vector defining the area of the loop. These expressions are equal to the ones obtained for an elastic dipole (8) and (9), with the equivalent dipole tensor of the dislocation loop given by

$$P_{jk} = -C_{jklm}\, b_m\, A_l. \tag{26}$$

Looking at the interaction with an external stress field, the interaction energy with the dislocation loop is given by

$$E^{\mathrm{int}} = \int_A \sigma_{ij}^{\mathrm{ext}}(\vec{r})\, b_i\, n_j\, \mathrm{d}A. \tag{27}$$

For an infinitesimal loop, it simply becomes

$$E^{\mathrm{int}} = \sigma_{ij}^{\mathrm{ext}}(\vec{0})\, b_i\, A_j, \tag{28}$$

which is equivalent to the expression (12) obtained for an elastic dipole when the equivalent dipole tensor of the dislocation loop is given by Eq. (26).

3.4. Polarizability

The equivalent point-forces distribution of a point-defect can be altered by an applied elastic field [17]. This applied elastic field thus leads to an induced elastic dipole and the total elastic dipole of the point-defect now depends on the applied strain $\varepsilon^{\mathrm{ext}}$:

$$P_{ij}(\varepsilon^{\mathrm{ext}}) = P_{ij}^0 + \alpha_{ijkl}\varepsilon_{kl}^{\mathrm{ext}}, \tag{29}$$

where P_{ij}^0 is the permanent elastic dipole in absence of applied strain and α_{ijkl} is the point-defect diaelastic polarizability [18–20]. Considering the analogy with the Eshelby's inclusion, this polarizability corresponds to an infinitesimal inhomogeneous inclusion, *i.e.* an inclusion with different elastic constants than the surrounding matrix. It describes the fact that the matrix close to the point-defect has a different elastic response to an applied strain because of the perturbations of the atomic bonding caused by the point-defect. For the analogy with an infinitesimal dislocation loop, the polarizability corresponds to the fact that the loop can change its shape by glide on its prismatic cylinder (or in its habit plane for a pure glide loop) under the action of the applied elastic field.

Following Schober [18], the interaction of a point-defect located at the origin with an applied strain is now given by

$$E^{\mathrm{int}} = -P_{ij}^0\, \varepsilon_{ij}^{\mathrm{ext}}(\vec{0}) - \frac{1}{2}\, \alpha_{ijkl}\, \varepsilon_{ij}^{\mathrm{ext}}(\vec{0})\, \varepsilon_{kl}^{\mathrm{ext}}(\vec{0}). \tag{30}$$

This expression of the interaction energy, which includes the defect polarizability, has important consequences for the modeling of point-defects as it shows that some coupling is possible between two different applied elastic fields. Considering the point-defect interaction with the two strain fields $\varepsilon^{(1)}$ and $\varepsilon^{(2)}$ originating from two different sources, the interaction energy is now given by

$$\begin{aligned} E^{\mathrm{int}} =& -P_{ij}^0 \left(\varepsilon_{ij}^{(1)} + \varepsilon_{ij}^{(2)}\right) \\ & - \frac{1}{2}\, \alpha_{ijkl} \left(\varepsilon_{ij}^{(1)} + \varepsilon_{ij}^{(2)}\right) \left(\varepsilon_{kl}^{(1)} + \varepsilon_{kl}^{(2)}\right), \\ =& -P_{ij}^0 \varepsilon_{ij}^{(1)} - \frac{1}{2}\, \alpha_{ijkl}\, \varepsilon_{ij}^{(1)}\, \varepsilon_{kl}^{(1)} \\ & - P_{ij}^0 \varepsilon_{ij}^{(2)} - \frac{1}{2}\, \alpha_{ijkl}\, \varepsilon_{ij}^{(2)}\, \varepsilon_{kl}^{(2)} \\ & - \alpha_{ijkl}\, \varepsilon_{ij}^{(1)}\, \varepsilon_{kl}^{(2)}. \end{aligned}$$

The last line therefore shows that, without the polarizability, the interaction energy of the point-defect with the two strain fields will be simply the superposition of the two interaction energies with each strain fields considered separately. A coupling is introduced only through the polarizability. Such a coupling is for instance at the origin of one of the

mechanisms proposed to explain creep under irradiation. Indeed, because of the polarizability, the interaction of point-defects, either vacancies or self-interstitial atoms, with dislocations under an applied stress depends on the dislocation orientation with respect to the applied stress. This stronger interaction with some dislocation families leads to a larger drift term in the diffusion equation of the point-defect and thus to a greater absorption of the point-defect by these dislocations, a mechanism known as Stress Induced Preferential Absorption (or SIPA) [21–24]. This polarizability is also the cause, in alloy solid solutions, of the variation of the matrix elastic constants with their solute content.

This diaelastic polarizability caused by the perturbation of the elastic response of the surrounding matrix manifests itself at the lowest temperature, even 0 K, and whatever the characteristic time of the applied strain. At finite temperature there may be another source of polarizability. If the point-defect can adopt different configurations, for instance different variants corresponding to different orientations of the point-defect like for a carbon interstitial atom in a body-centered cubic Fe matrix, then the occupancy distribution of these configurations will be modified under an applied stress or strain. This possible redistribution of the point-defect gives rise to anelasticity [10], the most famous case being the Snoek relaxation in iron alloys containing interstitial solute atoms like C and N [25]. When thermally activated transitions between the different configurations of the point-defect are fast enough compared to the characteristic time of the applied stress, the distribution of the different configurations corresponds to thermal equilibrium. Assuming that all configurations have the same energy in a stress-free state and denoting by P_{ij}^{μ} the elastic dipole of the configuration μ, the average dipole of the point-defect is then given by

$$\langle P_{ij} \rangle = \frac{\sum_{\mu} \exp\left(P_{kl}^{\mu} \varepsilon_{kl}^{\mathrm{ext}} \,/\, kT\right) P_{ij}^{\mu}}{\sum_{\mu} \exp\left(P_{kl}^{\mu} \varepsilon_{kl}^{\mathrm{ext}} \,/\, kT\right)}.$$

As a consequence, the average elastic dipole of the point-defect distribution is now depending on the applied stress and on the temperature, an effect known as paraelasticity [17]. At temperatures high enough to allow for transition between the different configurations, the interaction energy of the configurations with the applied strain is usually small compared to kT. One can make a series expansion of the exponentials to obtain

$$\langle P_{ij} \rangle = \frac{1}{n_{\mathrm{v}}} \sum_{\mu=1}^{n_{\mathrm{v}}} P_{ij}^{\mu} - \left(\frac{1}{{n_{\mathrm{v}}}^2} \sum_{\mu,\nu=1}^{n_{\mathrm{v}}} P_{ij}^{\mu} P_{kl}^{\nu} - \frac{1}{n_{\mathrm{v}}} \sum_{\mu=1}^{n_{\mathrm{v}}} P_{ij}^{\mu} P_{kl}^{\mu} \right) \frac{\varepsilon_{kl}^{\mathrm{ext}}}{kT},$$

where n_{v} is the number of configurations. This leads to the same linear variation of the elastic dipole with the applied strain as for the diaelastic polarizability (Eq. 29), except that the paraelastic polarizability is depending on the temperature.

4. Parameterization of elastic dipoles

To properly model a point-defect with continuum elasticity theory, one only needs to know its elastic dipole. It is then possible to describe the elastic displacement (Eq. 8) or the stress field (Eq. 9) induced by the point-defect, and also to calculate its interaction with an external elastic field (Eq. 12). This elastic dipole can be determined either using atomistic simulations or from experiments.

4.1. From atomistic simulations

Different strategies can be considered for the identification of elastic dipoles in atomistic simulations. This elastic dipole can be directly deduced from the stress existing in the simulation box, or from a fit of the atomic displacements, or finally from a summation of the Kanzaki forces. We examine here these three techniques and discuss their merits and drawbacks.

Definition from the stress

Let us consider a simulation box of volume V, the equilibrium volume of the pristine bulk material. We introduce one point-defect in the simulation box and assume periodic boundary conditions to preclude any difficulty associated with surfaces. Elasticity theory can be used to predict the variation of the energy of the simulation box submitted to a homogeneous strain ε. Using the interaction energy of a point-defect with an external strain given in Eq. (12), one obtains

$$E(\varepsilon) = E_0 + E^{\mathrm{PD}} + \frac{V}{2} C_{ijkl} \varepsilon_{ij} \varepsilon_{kl} - P_{ij} \varepsilon_{ij}, \quad (31)$$

with E_0 the bulk reference energy and E^{PD} the point-defect energy, which can contain a contribution from the interactions of the point-defect with

its periodic images (see section 5.4). The average residual stress on the simulation box is obtained by simple derivation as[3]

$$\begin{aligned}\langle\sigma_{ij}(\varepsilon)\rangle &= \frac{1}{V}\frac{\partial E}{\partial\varepsilon_{ij}},\\ &= C_{ijkl}\varepsilon_{kl} - \frac{1}{V}P_{ij}.\end{aligned} \tag{32}$$

In the particular case where the periodicity vectors are kept fixed between the defective and pristine supercells ($\varepsilon = 0$), the elastic dipole is proportional to the residual stress weighted by the supercell volume:

$$P_{ij} = -V\langle\sigma_{ij}\rangle. \tag{33}$$

This residual stress corresponds to the stress increase, after atomic relaxation, due to the introduction of the point-defect into the simulation box. When this equation is used to determine the elastic dipole in *ab initio* calculations, one should pay attention to the spurious stress which may exist in the equilibrium perfect supercell because of finite convergence criteria of such calculations. This spurious stress has to be subtracted from the stress of the defective supercell, so the residual stress entering Eq. 33 is only the stress increment associated with the introduction of the point-defect.

One can also consider the opposite situation where a homogeneous strain $\bar{\varepsilon}$ has been applied to cancel the residual stress. The elastic dipole is then proportional to this homogeneous strain:

$$P_{ij} = VC_{ijkl}\bar{\varepsilon}_{kl}. \tag{34}$$

One would nevertheless generally prefer working with fixed periodicity vectors ($\varepsilon = 0$) as $\sigma = 0$ calculations necessitate an increased number of force calculations, as well as an increased precision for *ab initio* calculations. In the more general case where a homogeneous strain is applied and a residual stress is observed, the elastic dipole can still be derived from these two quantities using Eq. (32).

This definition of the elastic dipole from the residual stress (Eq. 33), or more generally from both the applied strain and the residual stress (Eq. 32), is to be related to the dipole tensor measurement first proposed by Gillan [28, 29], where the elastic dipole is equal to the strain derivative of the formation energy, evaluated at zero strain. Instead of doing this derivative numerically, one can simply use the analytical derivative, *i.e.* the stress on the simulation box, which is a standard output of any atomistic simulations code, including *ab initio* calculations. This technique to extract elastic dipoles from atomistic simulations has been validated [30–32], through successful comparisons of interaction energies between point-defects with external strain fields, as given by direct atomistic simulations and as given by the elasticity theory predictions using the elastic dipole identified through Eq. (33). The residual stress therefore leads to quantitative estimates of the elastic dipoles.

Definition from the displacement field

The elastic dipole can also be obtained from the displacement field, as proposed by Chen *et al.* [33]. Using the displacement field $\vec{u}^{\text{at}}(\vec{R})$ obtained after relaxation in atomistic simulations, a least-square fit of the displacement field $\vec{u}^{\text{el}}(\vec{R})$ predicted by elasticity theory can be realized, using the dipole components of the dipole as fit variables. A reasonable cost function for the least-square fit is

$$f(P_{ij}) = \sum_{\substack{\vec{R}\\ \|\vec{R}\|>r_{\text{excl}}}} \left\| R^2\left[\vec{u}^{\text{el}}(\vec{R}) - \vec{u}^{\text{at}}(\vec{R})\right]\right\|^2, \tag{35}$$

with r_{excl} the radius of a small zone around the point-defect, so as to exclude from the fit the atomic positions where elasticity does not hold. The R^2 factor accounts for the scaling of the displacement field with the distance to the point-defect, thus giving a similar weight to all atomic positions included into the fit. For atomistic simulations with periodic boundary conditions, one needs to superimpose the elastic displacements of the point-defect with its periodic images, which can be done by simple summation, taking care of the conditional convergence of the corresponding sum [32]. With large simulation boxes ($\geq$ 1500 atoms), the obtained elastic dipole components agree with the values deduced from the residual stress, and the choice of r_{excl} is not critical. The number of atomic positions included in the fit, and for which elasticity is valid, is sufficiently high to avoid issues arising from the defect core zone [32]. In contrast, for small simulation boxes of a few hundred atoms, *i.e.* typical of *ab initio* simulations, the obtained P_{ij} values are highly sensitive to r_{excl}, and their convergence with r_{excl} cannot be guaranteed. This fit of the displacement field appears therefore impractical to obtain precise values of the elastic dipole in *ab initio* calculations.

[3] See also Refs. [26] and [27] for other proofs.

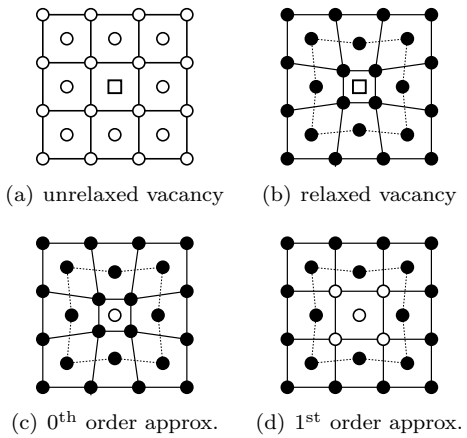

Figure 1: Procedure for the computation of the Kanzaki forces in the case of a vacancy. The white spheres correspond to atoms at their perfect bulk positions, *i.e.* before relaxation, the white square to the vacancy, and the black spheres to the atoms at their relaxed position around the defect.

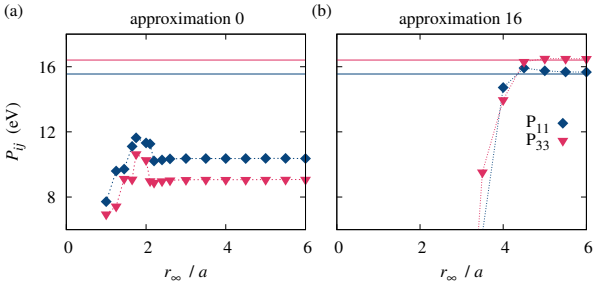

Figure 2: Elastic dipole components of the SIA octahedral configuration in hcp Zr, as a function of the cutoff radius r_∞ of the force summation normalized by the lattice parameter a. Values are obtained by the Kanzaki's forces approach on a simulation box containing 12800 atoms, restoring (a) only the point-defect, and (b) up to 16 defect neighbor shells. The horizontal lines are the values deduced from the residual stress. Calculations have been performed with the EAM #3 potential of Ref. [42] (see Ref. [32] for more details).

Definition from the Kanzaki forces

The definition given in Eq. (10) of the elastic dipole as the first moment of the point-force distribution offers a third way to extract this elastic dipole from atomic simulations. This corresponds to the Kanzaki force method [8, 34–41]. Kanzaki forces are defined as the forces which have to be applied to the atoms in the neighborhood of the point-defect to produce the same displacement field in the pristine crystal as in the defective supercell. Computation of these Kanzaki forces can be performed following the procedure given in Ref. [39], which is illustrated for a vacancy in Fig. 1. Starting from the relaxed structure of the point-defect (Fig. 1b), the defect is restored in the simulation cell, *e.g.* the suppressed atom is added back for the vacancy case (Fig. 1c). A static force calculation is performed then and provides the opposite of the searched forces on all atoms in the obtained simulation cell. These atomic forces are used to compute the elastic dipole $P_{ij} = \sum_q F_j^q a_i^q$, with $\vec{F}^q$ the opposite of the force acting on atom at $\vec{a}^q$, assuming the point-defect is located at the origin. The summation is usually restricted to atoms located inside a sphere of radius r_∞.

As Kanzaki's technique is valid only in the harmonic approximation, one checks that the atomic forces entering the elastic dipole definition are in the harmonic regime by restoring larger and larger defect neighboring shells to their perfect bulk positions [39] (Fig. 1c-d), computing the forces on the obtained restored structures, and then the elastic dipole. The case where n defect neighbor shells are restored is referred to as the n^{th} order approximation. As the restored zone becomes larger, the atoms remaining at their relaxed positions are more likely to sit in an harmonic region. The convergence of the resulting elastic dipole components with respect to n thus enables to evaluate the harmonicity aspect.

Fig. 2 provides the elastic dipole values as a function of the cutoff radius r_∞, for the octahedral configuration of the self-interstitial atom (SIA) in hcp Zr. Only the point-defect has been restored in Fig. 2a (approximation 0), whereas the restoration zone extends to the 16$^{\text{th}}$ nearest-neighbors in Fig. 2b. Constant P_{ij} values are reached for a cutoff radius $r_\infty \sim 2.5\,a$ and $\sim 4\,a$, respectively, showing that the defect-induced forces are long-ranged [32, 41]. As a result, the supercell needs to be large enough to avoid convolution of the force field by periodic boundary conditions and a high precision on the atomic forces is required. Comparing with the elastic dipole deduced from the residual stress, one cannot only restore the point-defect (approximation 0 in Fig. 2a) to obtain a quantitative estimate with the Kanzaki method. A restoration zone extending at least to the 16$^{\text{th}}$ nearest neighbors is necessary for this point-defect to obtain the correct elastic dipole. As the anharmonic region depends on the defect and on the material, one cannot choose *a pri-*

ori a radius for the restoration zone, but one needs to check the convergence of the elastic dipole with the size of this restoration zone.

Discussion

These three approaches lead to the same values of the elastic dipole when large enough supercells are used, thus confirming the consistency of this elastic description of the point-defect. This has been checked in Ref. [32] for the vacancy and various configurations of the SIA in hcp Zr. But for small simulation cells typical of *ab initio* calculations, both the fit of the displacement field and the calculation from the Kanzaki forces are usually not precise enough because of the too large defect core region, *i.e.* the region which has to be excluded from the displacement fit or the restoration zone for the Kanzaki forces. This is penalizing for *ab initio* calculations, even for point-defects as simple as the H solute or the vacancy in hcp Zr [32, 43]. Besides, the Kanzaki's technique requires additional calculations to obtain the defect-induced forces and to check that the forces entering the dipole definition are in the harmonic regime. As this restoration zone is extended, the defect-induced forces become smaller and the precision has to be increased. The definition from the residual stress appears indeed as the only method leading to reliable P_{ij} values within *ab initio* simulations. It is also easy to apply, as it does not require any post treatment nor additional calculations: it only uses the homogeneous stress on the simulation box and the knowledge of the defect position is not needed.

All these methods can be of course also used to determine the diaelastic polarizability. One only needs to get the elastic dipole for various applied strains. The linear equation (29) then leads the stress-free elastic dipole P^0_{ij} and the polarizability α_{ijkl}. The most convenient method remains a definition from the residual stress. Considering the polarizability, Eq. (32) now writes

$$\langle \sigma_{ij}(\varepsilon) \rangle = \left(C_{ijkl} - \frac{1}{V} \alpha_{ijkl} \right) \varepsilon_{kl} - \frac{1}{V} P_{ij}, \quad (36)$$

thus showing that the polarizability is associated with a variation of the elastic constants proportional to the point-defect volume fraction. This linear variation of the elastic constants arising from the point-defect polarizability has been characterized for vacancies and SIAs in face-centered cubic (fcc) copper [44], or various solute atoms in body-centered cubic (bcc) iron [45, 46].

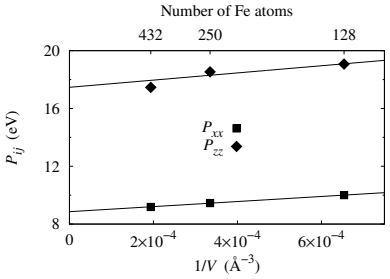

Figure 3: Elastic dipole of a C atom lying in a [001] octahedral interstitial site in bcc Fe as a function of the inverse volume V of the supercell. The elastic dipole has been deduced from the residual stress in *ab initio* calculations (see Ref. [47] for more details).

One consequence of the diaelastic polarizability is that the elastic dipole may depend on the size of the supercell with periodic boundary conditions. The strain at the point-defect position is indeed the superposition of the homogeneous strain ε_{ij} and the strains created by the periodic images of the point-defect $\varepsilon^{\mathrm{p}}_{ij}$. In the $\varepsilon = 0$ case for instance, the obtained elastic dipole is then

$$P_{ij} = P^0_{ij} + \alpha_{ijkl} \varepsilon^{\mathrm{p}}_{kl}. \quad (37)$$

As the strain created by a point-defect varies as the inverse of the cube of the separation distance (Eq. 9), the last term in Eq. (37) scales with the inverse of the supercell volume. Therefore, when homothetic supercells are used, one generally observes the following volume variation

$$P_{ij} = P^0_{ij} + \frac{\delta P_{ij}}{V},$$

which can be used to extrapolate the elastic dipole to an infinite volume, *i.e.* to the dilute limit [26, 32, 47]. An example of this linear variation with the inverse volume is shown in Fig. 3 for an interstitial C atom in a bcc Fe matrix.

4.2. From experiments

From an experimental perspective, when trying to extract elastic dipole of point-defects, both the symmetry and the magnitude of the components of the elastic dipole tensor are *a priori* unknown, and possibly also the number of defect-types into the material. We first restrict ourselves to the case where only one single type of point-defect with a known symmetry is present.

If the point-defect has a lower symmetry than the host crystal, then it can adopt several variants

which are equivalent by symmetry but possess different orientations. The energy of such a volume V containing different variants of the point-defect and submitted to a homogeneous strain is

$$E(\varepsilon) = E_0 + E^{\mathrm{PD}} + \frac{V}{2} C_{ijkl}\varepsilon_{ij}\varepsilon_{kl} - V\sum_{\mu=1}^{n_\mathrm{v}} c_\mu P^\mu_{ij}\varepsilon_{ij}, \quad (38)$$

with n_v the total number of different variants and c_μ the volume concentration of variant μ. This relation assumes that the different point-defects are not interacting, which is valid in the dilute limit. For zero stress conditions, as usually the case in experiments, the average strain induced by this assembly of point-defects is

$$\bar{\varepsilon}_{ij} = S_{ijkl}\sum_{\mu=1}^{n_\mathrm{v}} c_\mu P^\mu_{kl}, \quad (39)$$

with S_{ijkl} the inverse of the elastic constants C_{ijkl}. This linear relation between the strain and the point-defect concentrations corresponds to a Vegard's law and allows for many connections with experiments. It generalizes Eq. 34 to the case of a volume containing a population of the same point-defect with different variants. As mentioned in §3.1, point-defects in experiments are sometimes rather characterized by their λ-tensor [10]. Combining the definition of this λ-tensor (Eq. 13) with Eq. (39), one shows the equivalence of both definitions:

$$\lambda^\mu_{ij} = \frac{1}{\Omega_\mathrm{at}} S_{ijkl}\, P^\mu_{kl},$$

or equivalently Eq. (14).

When the point-defect has only one variant or when only one variant is selected by breaking the symmetry – through either a phase transformation (*e.g.* martensitic [48, 49]) or the interaction with an applied strain field for instance – the variations of the material lattice constants with the defect concentration follow the defect symmetry. If the point-defect concentration is known, the elastic dipole components are therefore fully accessible by measuring lattice parameter variations, *e.g.* by dilatometry or X-ray diffraction using the Bragg reflections.

On the other hand, for a completely disordered solid solution of point-defects with various variants ($n_\mathrm{v} > 1$), the average distortion induced by the point-defect population does not modify the parent crystal symmetry [10]. Each variant is equiprobable, *i.e.* $c_\mu = c_0/n_\mathrm{v}$ with c_0 the nominal point-defect concentration. The stress-free strain induced by the point-defect (Eq. 39) thus becomes

$$\bar{\varepsilon}_{ij} = c_0\, S_{ijkl}\,\langle P_{kl}\rangle \quad \text{with} \quad \langle P_{kl}\rangle = \frac{1}{n_\mathrm{v}}\sum_{\mu=1}^{n_\mathrm{v}} P^\mu_{kl}.$$

Measurements of the lattice parameter variations with the total defect concentration give thus access only to some sets of combinations of the P_{ij} components. For instance, if we consider a point-defect in a cubic crystal, like a C solute in an octahedral site of a bcc Fe crystal, one obtains the following variation of the lattice parameter with the solute concentration

$$a(c_0) = a_0\left(1 + \frac{\mathrm{Tr}\,(P)}{3\,(C_{11}+2C_{12})}\, c_0\right), \quad (40)$$

with C_{11} and C_{12} the elastic constants in Voigt notation. This variation can again be characterized using dilatometry or X-ray diffraction. But knowing $\mathrm{Tr}\,(P)$ is not sufficient for a point-defect with a lower symmetry than the cubic symmetry of the crystal, as the elastic dipole has several independent components (two for the C solute atom in bcc Fe). Additional information is therefore needed to fully characterize the point-defect.

For those defects having a lower symmetry than their parent crystal, the anelastic relaxation experiments may provide such supplementary data [10, 50]. By applying an appropriate stress, a splitting of the point-defect energy levels occurs, and a redistribution of the defect populations is operated. The relaxation of the compliance moduli then gives access to other combinations of the elastic dipole components. Not all of the relaxations are allowed by symmetry, as illustrated for the C solute in bcc Fe, where only the quantity $|P_{11} - P_{33}|$ is accessible [51]. The number of parameters accessible from anelastic measurements is lower than the independent components of the defect elastic dipole. This technique must then be used in combination with other measurements, like the variations of the lattice parameter.

Alternatively, a useful technique working with a random defect distribution is the diffuse Huang scattering. The diffuse scattering of X-rays near Bragg reflections [52–54] reflects the distortion scattering caused by the long-range part of the defect-induced displacement field. It thus provides information about the strength of the point-defect elastic dipole. The scattered intensity is proportional –

in the dilute limit – to the defect concentration and to a linear combination of quadratic expressions of the elastic dipole components. The coefficients of this combination are functions of the crystal elastic constants and of the scattering vector in the vicinity of a given reciprocal lattice vector. Therefore, by an appropriate choice of the relative scattering direction, the quadratic expressions can be determined separately.

Except for simple point-defects like a substitutional solute atom or a single vacancy, the defect symmetry may be unknown. Both anelastic relaxation and Huang scattering experiments provide important information for the determination of the defect symmetry. The presence of relaxation peaks in anelasticity is a direct consequence of the defect symmetry [10, 50]. Within Huang scattering experiments, information about the defect symmetry is obtained either by the analysis of the morphology of iso-intensity curves or through an appropriate choice of scattering directions to measure the Huang intensity.

To conclude, when extracting elastic dipoles from experiments, one must usually rely on a combination of several experimental techniques to obtain all components.

5. Some applications

5.1. Solute interaction with a dislocation

This elastic modeling can be used for instance to describe the interaction of a point-defect with other structural defects. To illustrate, and also validate, this approach, we consider a C interstitial atom interacting with a dislocation in a bcc iron matrix. This interstitial atom occupies the octahedral sites of the bcc lattice. As these sites have a tetragonal symmetry, the elastic dipole P_{ij} of the C atoms has two independent components and gives thus rise to both a size and a shape interaction. The interaction energy of the C atom with a dislocation is given by Eq. (12) where the external strain $\varepsilon_{ij}^{\text{ext}}$ is the strain created by the dislocation at the position of the C atom. This has been compared in Ref. [55] to direct results of atomistic simulations, using for the C elastic dipole and for the elastic constants the values given by the empirical potential used for the atomistic simulations. Results show that elastic theory leads to a quantitative prediction when all ingredients are included in the elastic model, *i.e.* when elastic anisotropy is taken into account to calculate the strain field created by the dislocation and

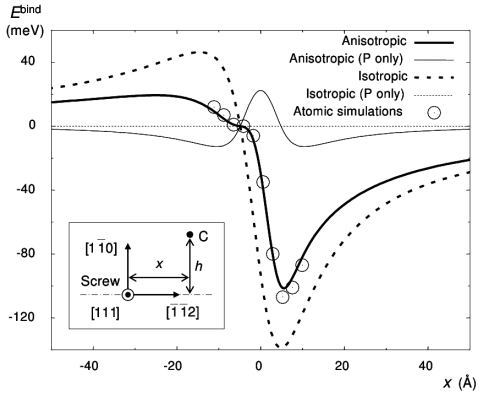

(a) Screw dislocation ($h = 4d_{110} \simeq 8.1\,\text{Å}$)

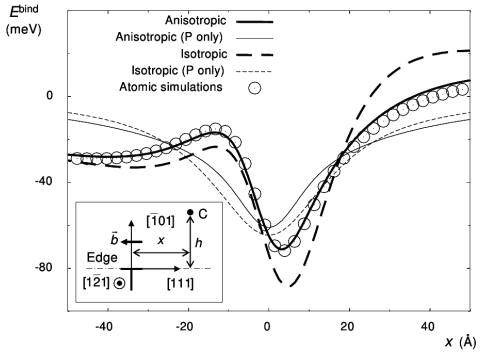

(b) Edge dislocation ($h = -9d_{110} \simeq -18.2\,\text{Å}$)

Figure 4: Binding energy $E^{\text{bind}} = -E^{\text{int}}$ between a screw or an edge dislocation and a C atom in bcc iron for different positions x of the dislocation in its glide plane. The C atom is lying in a [100] octahedral interstitial site at a fixed distance h of the dislocation glide plane. Symbols correspond to atomistic simulations and lines to elasticity theory, considering all components of the stress created by the dislocation or only the pressure, and using isotropic or anisotropic elasticity.

when both the dilatation and the tetragonal distortion induced by the C atom are considered (Fig. 4). The agreement between both techniques is perfect except when the C atom is in the dislocation core. With isotropic elasticity, the agreement with atomistic simulations is only qualitative, and when the shape interaction is not considered, *i.e.* when the C atom is modeled as a simple dilatation center ($P_{ij} = P\,\delta_{ij}$), elastic theory fails to predict this interaction (Fig. 4). The same comparison between atomistic simulations and elasticity theory has been performed for a vacancy and a SIA interacting with a screw dislocation still in bcc iron [41]. The agreement was not as good as for the C atom. But in this work, the elastic dipoles of the point-defects were

obtained from the Kanzaki forces, using the 0^{th} order approximation, which is usually not as precise as the definition from the stress (*cf.* § 4.1) and may explain some of the discrepancies.

One can also use elasticity theory to predict how the migration barriers of the point-defect are modified by a strain field. The migration energy is the energy difference between the saddle point and the stable position. Its dependence with an applied strain field $\varepsilon(\vec{r})$ is thus described by

$$E^{\text{m}}[\varepsilon] = E_0^{\text{m}} + P_{ij}^{\text{ini}}\varepsilon_{ij}(\vec{r}_{\text{ini}}) - P_{ij}^{\text{sad}}\varepsilon_{ij}(\vec{r}_{\text{sad}}), \quad (41)$$

where P_{ij}^{ini} and P_{ij}^{sad} are the elastic dipoles of the point-defect respectively at its initial stable position $\vec{r}_{\text{ini}}$ and at the saddle point $\vec{r}_{\text{sad}}$, and E_0^{m} is the migration energy without elastic interaction. Still for a C atom interacting with a dislocation in a bcc Fe matrix, comparison of this expression with results of direct atomistic simulations show a good agreement [56], as soon as the C atom is far enough from the dislocation core. Similar conclusions, on the validity of equation (41) to describe the variation of the solute migration energy with an applied strain, have been reached for a SIA diffusing in bcc Fe [33], a vacancy in hcp zirconium [30] or a Si impurity in fcc nickel [31].

5.2. Elastodiffusion

This simple model predicting the variation of the migration energy with an applied strain field (Eq. 41) can be used to study elastodiffusion. Elastodiffusion refers to the diffusion variations induced by an elastic field [57], either externally applied or internal through the presence of structural defects. Important implications exist for materials, such as transport and segregation of point-defects to dislocations leading to the formation of Cottrell atmospheres [58], irradiation creep [59], or anisotropic diffusion of dopants in semiconductor thin films [60, 61].

At the atomic scale, solid state diffusion occurs through the succession of thermally activated atomic jumps from stable to other stable positions, with atoms jumping either on vacancy sites or on interstitial sites of the host lattice. Within transition state theory [62], the frequency of such a transition is given by

$$\Gamma_\alpha = \nu_\alpha^0 \exp\left(-E_\alpha^{\text{m}} / kT\right), \quad (42)$$

where ν_α^0 is the attempt frequency for the transition α and E_α^{m} is the migration energy.

Considering the effect of a small strain field on this bulk system, the diffusion network and the site topology will not be modified. On the other hand, the presence of this small strain field modifies the migration energies and the attempt frequencies. As shown in the previous section, the elastic dipole description of the point-defect can predict the modification of the stable and saddle point energies, and thus of the migration energy (Eq. 41). Ignoring the strain effect on attempt frequencies, the incorporation of the modified energy barriers into stochastic simulations like atomistic or object kinetic Monte Carlo (OKMC) methods enables to characterize the point-defect elastodiffusion effect. This approach has been used, for instance, to study the directional diffusion of point-defects in the heterogeneous strain field of a dislocation, corresponding to a biased random walk [30, 56, 63].

Diffusion in a continuous solid body is characterized by the diffusion tensor D_{ij} which expresses the proportionality between the diffusion flux and the concentration gradient (Fick's law). The effect of an applied strain is then described by the elastodiffusion fourth-rank tensor d_{ijkl} [57], which gives the linear dependence of the diffusion tensor with the strain:

$$D_{ij} = D_{ij}^0 + d_{ijkl}\,\varepsilon_{kl}. \quad (43)$$

This elastodiffusion tensor obeys the minor symmetries $d_{ijkl} = d_{jikl} = d_{ijlk}$, because of the symmetry of the diffusion and deformation tensors, and also the crystal symmetries. Starting from the atomistic events as defined by their transition frequencies (Eq. 42), the diffusion coefficient, and its variation under an applied strain, can be evaluated from the long time evolution of the point-defect trajectories in stochastic simulations [64]. Alternatively, analytical approaches can be developed to provide expressions [65, 66]. The elastodiffusion can thus be computed by a perturbative approach, starting from the analytical expression of the diffusion tensor [57, 67]. This results in two different contributions: a geometrical contribution caused by the overall change of the jump vectors and a contribution due to the change in energy barriers as described by Eq. (41). This last contribution is thus a function of the elastic dipoles at the saddle point and stable positions. It is found to have an important magnitude in various systems [57, 67], being for instance notably predominant for interstitial impurities in hcp Mg [68]. It is temperature-dependent, sometimes leading to complex variations with non-

monotonic variations and also sign changes for some of its components [68]. As noted by Dederichs and Schroeder [57], the elastic dipole at the saddle point completely determines the stress-induced diffusion anisotropy in cubic crystals. Experimental measurement of the elastodiffusion tensor components can therefore provide useful information about the saddle point configurations.

Both approaches, relying either on stochastic simulations or analytical models, are now usually informed with *ab initio* computed formation and migration energies, and attempt frequencies. The elastic modeling of a point-defect through its elastic dipole offers thus a convenient way to transfer the information about the effects of an applied strain, as obtained from atomistic simulations, to the diffusion framework.

5.3. Bias calculations

Point-defect diffusion and absorption by elements of the microstructure such as dislocations, cavities, grain boundaries and precipitates play an important role in the macroscopic evolution of materials. It is especially true under irradiation, since in this case not only vacancies but also self-interstitial atoms (SIAs) migrate to these sinks. Owing to their large dipole tensor components, SIAs generally interact more than vacancies with the stress fields generated by sinks. This leads to a difference in point-defect fluxes to a given sink known as the "absorption bias". For example, in the "dislocation bias model" [69], which is one of the most popular models to explain irradiation void swelling, dislocations are known as biased sinks: they absorb more interstitials than vacancies. Voids, which produce shorter range stress fields, are considered as neutral sinks, meaning that their absorption bias is zero. Since SIAs and vacancies are produced in the same quantity, the preferential absorption of SIAs by dislocations leads to a net flux of vacancies to voids and thus to void growth. Similar explanations based on absorption biases have been given to rationalize irradiation creep [21] and irradiation growth in hexagonal materials [70]. In order to predict the kinetics of such phenomena, a precise evaluation of absorption biases is necessary.

Following the rate theory formalism [69], the absorption bias of a given sink can be written as the relative difference of sink strengths for interstitials (k_i^2) and vacancies (k_v^2) [71]. The strength of a sink for a point-defect θ ($\theta = i, v$) is related to the loss rate ϕ_θ through

$$\phi_\theta = k_\theta^2 D_\theta c_\theta, \tag{44}$$

where D_θ is the diffusion coefficient free of elastic interactions and c_θ is the volume concentration of θ.

The sink strength can be calculated with different methods, for example by solving the diffusion equation around the sink [57, 69] or an associated phase field model [72], or by performing object kinetic Monte Carlo simulations (OKMC) [73, 74]. It should be noted that analytical solution of the diffusion equation is limited to a few cases and often requires the defect properties or the stress field to be simplified [75–77], so in general numerical simulations are necessary [78–81]. In the following we consider the OKMC approach, due to its simplicity and its flexibility to introduce complex diffusion mechanisms and the effect of stress fields [30, 82, 83].

In OKMC simulations of sink strengths, a sink is introduced in a simulation box where periodic boundary conditions are used and point-defects are generated at a given rate K. They diffuse in the box by successive atomic jumps until they are absorbed by the sink. For each defect in the simulation box, the jump frequencies of all jumps from the current stable state to the possible final states are calculated and the next event is chosen according to the standard residence time algorithm [84, 85]. The jump frequency of event α is given by Eq. (42), considering the strain dependence of the migration energy through Eq. (41).

The sink strength is deduced from the average number of defects in the box $\overline{N}_\theta$ at steady state by the following equation [83]:

$$k_\theta^2 = \frac{K}{D_\theta \overline{N}_\theta}, \tag{45}$$

from which the bias is deduced:

$$B = \frac{k_i^2 - k_v^2}{k_i^2}. \tag{46}$$

Another method is often used for the calculation of sink strengths with OKMC [73, 74]. For each defect, the number of jumps it performs before it is absorbed by the sink is registered. The sink strength is then deduced from the average number of jumps. Although this method is equivalent to the method based on the average concentration in the non-interacting case, it is no more valid if elastic interactions are included. In this case the

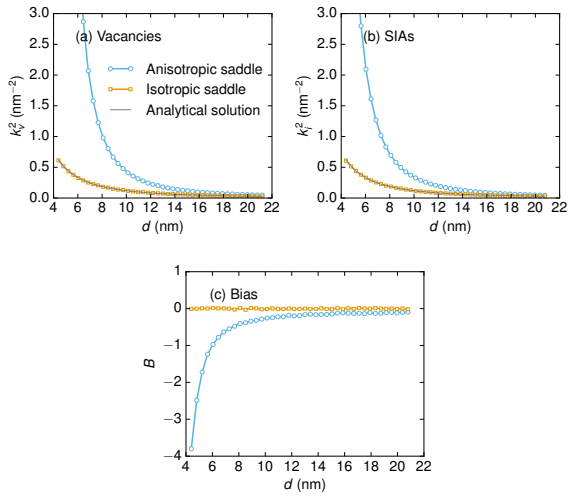

Figure 5: Sink strengths of a twist grain boundary ($\theta = 7.5°$) for (a) vacancies and (b) SIAs, and (c) absorption bias, as a function of the layer thickness d. (see Ref. [83] for more details).

average time before absorption should be measured instead of the average number of jumps, since jump frequencies now depend on the location of the defect and are usually higher. Therefore, applying this method in the interacting case often leads to an underestimation of sink strengths.

As an illustration, we consider the study published in Ref. [83], where sink strengths of semi-coherent interfaces have been calculated with OKMC, taking into account the effect of the strain field generated by the interfaces. The strain is the sum of the coherency strain and of the strain due to interface dislocations. It has been calculated by a semi-analytical method within the framework of anisotropic elasticity [83, 86, 87]. We consider the case of a twist grain boundary in Ag, which produces a purely deviatoric strain field. Two grain boundaries distant from each other by d are introduced in the box and periodic boundary conditions are applied.

Dipole tensors of vacancies and SIAs in Ag have been computed by DFT for both stable and saddle positions [83], using the residual stress definition (Eq. 33). At the ground state, the elastic dipole of the vacancy is isotropic and the one of the SIA almost isotropic. On the other hand, the elastic dipole tensors have a significant deviatoric component for both point-defects at their saddle point.

Sink strengths of the twist grain boundary are shown in Fig. 5-(a,b) as a function of the layer thickness d and compared to the analytical result with no elastic interactions $k^2 = 12/d^2$. Sink strengths for both vacancies and SIAs are significantly increased when elastic interactions are included and when anisotropy at saddle point is taken into account, especially for thinner layers. However, if the saddle point is considered isotropic, the non-interacting case is recovered. This is due to the deviatoric character of the strain field: since the dipole tensor of the vacancy in its ground state is purely hydrostatic, the interaction energy of a vacancy with the strain field is zero and there is no thermodynamic driving force for the absorption of the vacancy. A similar result is obtained for SIAs, because of their almost purely hydrostatic dipole for their ground state. Fig. 5c shows the evolution of the bias. For this interface, saddle point anisotropy leads to a negative bias, meaning that vacancies tend to be more absorbed than interstitials.

This approach has also been recently used for the calculation of the sink strength of straight dislocations and cavities in aluminum [88]. In both cases, saddle point anisotropy appears to have a significant influence on the sink strengths. This confirms analytical results obtained with various levels of approximation [77, 89, 90].

5.4. Isolated defect in atomistic simulations

The elastic modeling of point-defects is also useful in the context of atomistic simulations. Such simulations, in particular *ab initio* calculations, are now unavoidable to obtain the point-defects energetics, like their formation and migration energies [1]. However, an ongoing issue is their difficulty to obtain the properties of isolated defects. One can use atomistic simulations with controlled surface to model an isolated point-defect [91–95], but then, the excess energy associated with the point-defect could be exactly set apart from the one of the external surfaces or interfaces only for interatomic potentials with a cutoff interaction radius, corresponding to short-range empirical potentials like EAM. For more complex potentials or for *ab initio* calculations, the absence of any interaction cutoff prevents an unambiguous definition of the point-defect energy. A supercell approach relying on periodic boundary conditions is therefore usually preferred. The combined effect of periodic boundary conditions and of the limited size of such calculations, for numerical cost reasons, makes the computed properties difficult to converge for defects inducing long-

range effects. This problem is well-known in the context of charged point-defects, where long-range Coulombian interactions exist between the defect and its periodic images and for which corrective schemes have been developed [96–98]. For neutral defects, interactions between periodic images also exist. These interactions are of elastic origin and decay like the inverse cube of the separation distance. Consequently, the computed excess energies are those of a periodic array of interacting point-defects, and converge with the inverse of the supercell volume to the energy of the isolated defect. This can be penalizing for defects inducing large distortions, like SIAs or clusters, or for atomic calculations where only small supercells are reachable. The elastic description of a point-defect allows calculating this spurious elastic interaction associated with periodic boundary conditions to obtain the energy properties of the isolated point-defect [99].

After atomic relaxation, the excess energy of a supercell containing one point-defect is given by:

$$E^{\mathrm{PD}}_{\mathrm{PBC}}(\bar{\varepsilon}=0) = E^{\mathrm{PD}}_{\infty} + \frac{1}{2}E^{\mathrm{int}}_{\mathrm{PBC}}, \qquad (47)$$

where E^{PD}_{∞} is the excess energy of the isolated defect and $E^{\mathrm{int}}_{\mathrm{PBC}}$ is the interaction energy of the defect with its periodic images. The factor $1/2$ arises because half of the interaction is devoted to the defect itself and the other goes to its periodic images. Continuous linear elasticity theory can be used to evaluate this elastic interaction. If the point-defect is characterized by the elastic dipole P_{ij}, following Eq. 12, this interaction energy is given by

$$E^{\mathrm{int}}_{\mathrm{PBC}} = -P_{ij}\,\varepsilon^{\mathrm{PBC}}_{ij}, \qquad (48)$$

with $\varepsilon^{\mathrm{PBC}}_{ij}$ the strain created by the defect periodic images. It can be obtained by direct summation

$$\varepsilon^{\mathrm{PBC}}_{ij} = -{\sum_{n,m,p}}' G_{ik,jl}(n\vec{a}_1 + m\vec{a}_2 + p\vec{a}_3)\,P_{kl}. \qquad (49)$$

with $\vec{a}_1$, $\vec{a}_2$ and $\vec{a}_3$ the periodicity vectors of the supercell. The prime sign indicates that the diverging term ($n = m = p = 0$) has been excluded from the sum. As the second derivative of the Green's function $G_{ik,jl}(\vec{r})$ is decaying like $1/r^3$, this sum is only conditionally convergent. It can be regularized following the numerical scheme proposed by Cai [100].

After computing the point-defect energy with an atomistic simulation code, this energy can be corrected by subtracting the interaction energy with the periodic images (Eq. 47) to obtain the properties of the isolated defect. This interaction energy is computed from the elastic constants of the perfect crystal, which are needed to evaluate the Green's function and its derivative (*cf.* § 2.3), and from the residual stress of the defective supercell to determine the point-defect elastic dipole (*cf.* § 4.1). This is therefore a simple post-treatment, which does not involve any fitting procedure and which can be performed using the ANETO program provided as supplemental material of Ref. [99].

We have assumed in Eq. (47) that the supercell containing the point-defect has the same periodicity vector than the perfect supercell, *i.e.* the applied homogenous strain $\bar{\varepsilon}$ is null. This corresponds to the easiest boundary conditions in atomistic simulations of point-defects. But sometimes, one prefers to relax also the periodicity vectors to nullify the stress in the supercell. Both these $\bar{\varepsilon}=0$ and $\sigma=0$ conditions converge to the same energy E^{PD}_{∞} in the thermodynamic limit but different energies are obtained for too small supercells. The elastic model can be further developed to rationalize this difference [26, 99]. For $\sigma=0$ conditions, a strain $\bar{\varepsilon}$ is applied to the defective supercell to nullify its stress. Eq. (47) therefore needs to be complemented with the energy contribution of this deformation

$$\Delta E(\bar{\varepsilon}) = \frac{V}{2}C_{ijkl}\bar{\varepsilon}_{ij}\bar{\varepsilon}_{kl} - P_{ij}\bar{\varepsilon}_{ij}.$$

This applied strain $\bar{\varepsilon}$ in zero stress calculations is linked to the elastic dipole by Eq. (34). The excess energy of the supercell containing one point-defect is thus now given by

$$\begin{aligned} E^{\mathrm{PD}}_{\mathrm{PBC}}(\sigma=0) &= E^{\mathrm{PD}}_{\infty} + \frac{1}{2}E^{\mathrm{int}}_{\mathrm{PBC}} - \frac{1}{2V}S_{ijkl}P_{ij}P_{kl} \\ &= E^{\mathrm{PD}}_{\mathrm{PBC}}(\bar{\varepsilon}=0) - \frac{1}{2V}S_{ijkl}P_{ij}P_{kl}, \end{aligned} \qquad (50)$$

where the elastic compliances of the bulk material S_{ijkl} are the inverse tensor of the elastic constants C_{ijkl}. This equation shows that $\bar{\varepsilon}=0$ and $\sigma=0$ conditions lead to point-defect excess energies differing by a factor proportional to the inverse of the supercell volume and to the square of the elastic dipole. This difference will be therefore important for small supercells and/or point-defects inducing an important perturbation of the host lattice. But once corrected through Eqs. (47) or (50), both approaches should lead to the same value. $\sigma=0$ calculations appear therefore unnecessary.

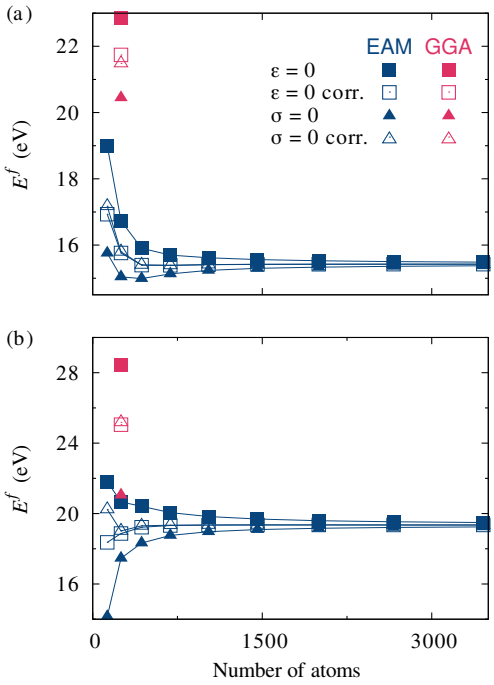

Figure 6: Formation energy of a SIA cluster containing eight interstitials in bcc iron calculated for fixed periodicity vectors ($\bar{\varepsilon} = 0$) or at zero stress ($\sigma = 0$) for different sizes of the simulation cell: (a) C15 aggregate and (b) parallel-dumbell configuration with a $\langle 111 \rangle$ orientation. Atomistic simulations are performed either with the M07 empirical potential [101] (EAM) or with *ab initio* calculations (GGA). Filled symbols refer to uncorrected results and open symbols to the results corrected by the elastic model (see Ref. [99] for more details).

We illustrate the usefulness of this elastic post-treatment on an atomistic study of SIA clusters in bcc iron. These clusters appear under irradiation and can adopt different morphologies [101]. In particular, some clusters can have a 3D structure with an underlying crystal symmetry corresponding to the C15 Laves' phase, and others have a planar structure corresponding to dislocation loop clusters with $1/2\,\langle 111 \rangle$ Burgers vectors.

The formation energies of two different configurations of a cluster containing 8 SIAs, a C15 aggregate and a planar aggregate of parallel-dumbells with a $\langle 111 \rangle$ orientation, are shown in Fig. 6 for different supercell sizes. They have been first calculated with an empirical EAM potential [101]: with fixed periodicity vectors ($\bar{\varepsilon} = 0$), one needs at least 2000 atoms for the C15 aggregate and 4000 atoms for the $\langle 111 \rangle$ planar configuration to get a formation energy converged to a precision better than 0.1 eV. The convergence is slightly faster for zero stress calculations ($\sigma = 0$) in the case of the C15 aggregate (Fig. 6a), but the opposite is true in the case of the $\langle 111 \rangle$ planar configuration (Fig. 6b). When we add the elastic correction, the convergence is improved for both cluster configurations. The corrected $\bar{\varepsilon} = 0$ and $\sigma = 0$ calculations lead then to the same formation energies, except for the smallest simulation cell (128 lattice sites) in the case of the $\langle 111 \rangle$ cluster. These formation energies have been also obtained with *ab initio* calculations for a simulation cell containing 250 lattice sites (Fig. 6). Uncorrected $\bar{\varepsilon} = 0$ calculations lead to an energy difference $\Delta E = -5.6\,\text{eV}$ between the C15 and the $\langle 111 \rangle$ planar configuration, whereas this energy difference is only $\Delta E = -0.6\,\text{eV}$ in $\sigma = 0$ calculations. This variation of the energy difference is rationalized once the elastic correction is added, and a good precision is obtained with this approach coupling *ab initio* calculations and elasticity theory, with an energy difference of $\Delta E = 3.5 \pm 0.2\,\text{eV}$. This elastic correction has been shown to accelerate the convergence of the point-defect formation and/or migration energies obtained from atomistic simulations, in particular from *ab initio* calculations, in numerous other cases like SIA in hcp Zr [99, 102], vacancy in diamond silicon [99], or solute interstitials in bcc iron [103].

6. Conclusions

Elasticity theory provides thus an efficient framework to model point-defects. Describing the point-defect as an equilibrated distribution of point-forces, the long range elastic field of the defect and its interaction with other elastic fields are fully characterized by the first moment of this force distribution, a second rank symmetric tensor called the elastic dipole. This description is equivalent to an infinitesimal Eshelby inclusion or an infinitesimal dislocation loop. Knowing only the elastic constants of the matrix and the elastic dipole, a quantitative modeling of the point-defect and its interactions is thus obtained. The value of this elastic dipole can be either deduced from experimental data, like Vegard's law parameters, or extracted from atomistic simulations. In this latter case, care must be taken to avoid finite-size effects, in particular for *ab initio* calculations. The definition through the residual stress appears as the most precise one to obtain the dipole tensors.

The elastic description offers a convenient framework to bridge the scales between an atomic and

a continuum description so as to consider the interaction of the point-defects with various complex elastic fields. This upscaling approach has already proven its efficiency in the modeling of elastodiffusion or in the calculation of absorption bias under irradiation. As the numerical evaluation of the elastic Green's function and its derivatives does not present nowadays any technical difficulty, such an elastic model offers also a nice route to simulate the evolution of a whole population of point-defects in a complex microstructure, considering their mutual interaction and their interaction with other structural defects, in the same spirit as dislocation dynamics simulations are now routinely used to model the evolution of a dislocation microstructure.

Acknowledgements - This work was performed using HPC resources from GENCI-CINES and -TGCC (Grants 2017-096847). The research was partly funded by the European Atomic Energy Community's (Euratom) Seventh Framework Program FP7 under grant agreement No. 604862 (MatISSE project) and in the framework of the EERA (European Energy Research Alliance) Joint Program on Nuclear Materials.

References

[1] C. Freysoldt, B. Grabowski, T. Hickel, J. Neugebauer, G. Kresse, A. Janotti, C. G. Van de Walle, First-principles calculations for point defects in solids, Rev. Mod. Phys. 86 (2014) 253—-305. doi:10.1103/revmodphys.86.253.

[2] J. Eshelby, The continuum theory of lattice defects, in: F. Seitz, D. Turnbull (Eds.), Solid State Physics, Vol. 3, Academic Press, 1956, pp. 79–144. doi:10.1016/S0081-1947(08)60132-0.

[3] L. D. Landau, E. M. Lifshitz, Theory of Elasticity, 2nd Edition, Vol. 7 of Course of Theoretical Physics, Pergamon Press, 1970.

[4] J. F. Nye, Physical Properties of Crystals - Their representation by tensors and matrices, Oxford University Press, 1957.

[5] D. M. Barnett, The precise evaluation of derivatives of the anisotropic elastic Green's functions, Phys. Status Solidi B 49 (1972) 741–748. doi:10.1002/pssb.2220490238.

[6] D. J. Bacon, D. M. Barnett, R. O. Scattergood, Anisotropic continuum theory of lattice defects, Prog. Mater. Sci. 23 (1980) 51–262. doi:10.1016/0079-6425(80)90007-9.

[7] R. Siems, Mechanical interactions of point defects, Phys. Status Solidi 30 (1968) 645–658. doi:10.1002/pssb.19680300226.

[8] G. Leibfried, N. Breuer, Point Defects in Metals I, Vol. 81 of Springer Tracts in Modern Physics, Springer-Verlag, Berlin, 1978. doi:10.1007/BFb0045966.

[9] C. Teodosiu, Elastic Models of Crystal Defects, Springer-Verlag, Berlin, 1982.

[10] A. S. Nowick, B. S. Berry, Anelastic Relaxation in Crystalline Solids, Academic Press, New York, 1972.

[11] J. D. Eshelby, The determination of the elastic field of an ellipsoidal inclusion, and related problems, Proc. Roy. Soc. Lond. A 241 (1957) 376–396. doi:10.1098/rspa.1957.0133.

[12] J. D. Eshelby, The elastic field outside an ellipsoidal inclusion, Proc. Roy. Soc. Lond. A 252 (1959) 561–569. doi:10.1098/rspa.1959.0173.

[13] M. Lazar, Micromechanics and theory of point defects in anisotropic elasticity: Eshelby factor meets Eshelby tensor, Journal of Micromechanics and Molecular Physics 02 (2017) 1750005. doi:10.1142/S2424913017500059.

[14] F. R. N. Nabarro, Theory of Crystal Dislocations, Oxford Univ. Press, London, 1967.

[15] T. Mura, Micromechanics of Defects in Solids, Kluwer Academic, Dordrecht, 1987.

[16] J. P. Hirth, J. Lothe, Theory of Dislocations, 2nd Edition, Wiley, New York, 1982.

[17] E. Kröner, Dia- and para-elasticity, in: F. Kroupa (Ed.), Theory of crystal defects, Academia, 1964, pp. 215–230.

[18] H. R. Schober, Polarizabilities of point defects in metals, J. Nucl. Mater. 126 (1984) 220–225. doi:10.1016/0022-3115(84)90032-1.

[19] M. P. Puls, C. H. Woo, Diaelastic polarizabilities due to vacancies and interstitials in metals, J. Nucl. Mater. 139 (1986) 48–59. doi:10.1016/0022-3115(86)90163-7.

[20] A. Granato, The temperature-independent component of the diaelastic effect, J. Alloys Compd. 211-212 (1994) 503–508. doi:10.1016/0925-8388(94)90553-3.

[21] P. T. Heald, M. V. Speight, Steady-state irradiation creep, Philos. Mag. 29 (1974) 1075–1080. doi:10.1080/14786437408226592.

[22] P. T. Heald, M. V. Speight, Point defect behaviour in irradiated materials, Acta Metall. 23 (1975) 1389–1399. doi:10.1016/0001-6160(75)90148-0.

[23] T. Bullough, J. R. Willis, The stress-induced point defect-dislocation interaction and its relevance to irradiation creep, Philos. Mag. 31 (1975) 855–861. doi:10.1080/14786437508229635.

[24] R. Bullough, M. Hayns, Irradiation-creep due to point defect absorption, J. Nucl. Mater. 57 (3) (1975) 348 – 352. doi:10.1016/0022-3115(75)90220-2.

[25] J. L. Snoek, Effect of small quantities of carbon and nitrogen on the elastic and plastic properties of iron, Physica 8 (1941) 711–733. doi:10.1016/S0031-8914(41)90517-7.

[26] B. Puchala, M. L. Falk, K. Garikipati, Elastic effects on relaxation volume tensor calculations, Phys. Rev. B 77 (2008) 174116. doi:10.1103/PhysRevB.77.174116.

[27] R. C. Pasianot, On the determination of defect dipoles from atomistic simulations using periodic boundary conditions, Philos. Mag. Lett. 96 (2016) 447–453. doi:10.1080/09500839.2016.1250965.

[28] M. J. Gillan, The volume of formation of defects in ionic crystals, Philos. Mag. A 43 (1981) 301–312. doi:10.1080/01418618108239410.

[29] M. J. Gillan, The long-range distortion caused by point defects, Philos. Mag. A 48 (1983) 903–919. doi:10.1080/01418618308244326.

[30] G. Subramanian, D. Perez, B. P. Uberuaga, C. N. Tomé, A. F. Voter, Method to account for arbi-

trary strains in kinetic Monte Carlo simulations, Phys. Rev. B 87 (2013) 144107. doi:10.1103/PhysRevB.87.144107.

[31] T. Garnier, V. R. Manga, P. Bellon, D. R. Trinkle, Diffusion of Si impurities in Ni under stress: A first-principles study, Phys. Rev. B 90 (2014) 024306. doi:10.1103/physrevb.90.024306.

[32] C. Varvenne, E. Clouet, Elastic dipoles of point defects from atomistic simulations, Phys. Rev. B 96 (2017) 224103. doi:10.1103/PhysRevB.96.224103.

[33] Z. Chen, N. Kioussis, N. Ghoniem, D. Seif, Strain-field effects on the formation and migration energies of self interstitials in alpha-Fe from first principles, Phys. Rev. B 81 (2010) 094102. doi:10.1103/PhysRevB.81.094102.

[34] H. Kanzaki, Point defects in face-centred cubic lattice — I Distortion around defects, J. Phys. Chem. Solids 2 (1957) 24 – 36. doi:10.1016/0022-3697(57)90003-3.

[35] I. D. Faux, A. B. Lidiard, The volume of formation of Schottky defects in ionic crystals, Zeitschrift für Naturforschung 26a (1971) 62–68.

[36] V. K. Tewary, Green-function method for lattice statics, Adv. Phys. 22 (1973) 757–810. doi:10.1080/00018737300101389.

[37] H. R. Schober, K. W. Ingle, Calculation of relaxation volumes, dipole tensors and kanzaki forces for point defects, J. Phys. F Metal. Phys. 10 (1980) 575–581. doi:10.1088/0305-4608/10/4/009.

[38] A. B. Lidiard, The volume of formation of schottky defects in ionic crystals, Philos. Mag. A 43 (1981) 291–300. doi:10.1080/01418618108239409.

[39] G. Simonelli, R. Pasianot, E. Savino, Point-defect computer simulation including angular forces in bcc iron, Phys. Rev. B 50 (1994) 727–738. doi:10.1103/PhysRevB.50.727.

[40] C. Domain, C. S. Becquart, J. Foct, Ab initio study of foreign interstitial atom (C, N) interactions with intrinsic point defects in alpha -Fe, Phys. Rev. B 69 (2004) 144112. doi:10.1103/PhysRevB.69.144112.

[41] E. Hayward, C. Deo, B. P. Uberuaga, C. N. Tomé, The interaction of a screw dislocation with point defects in bcc iron, Philos. Mag. 92 (2012) 2759–2778. doi:10.1080/14786435.2012.674646.

[42] M. I. Mendelev, G. J. Ackland, Development of an interatomic potential for the simulation of phase transformations in zirconium, Philos. Mag. Lett. 87 (2007) 349–359. doi:10.1080/09500830701191393.

[43] R. Nazarov, J. S. Majevadia, M. Patel, M. R. Wenman, D. S. Balint, J. Neugebauer, A. P. Sutton, First-principles calculation of the elastic dipole tensor of a point defect: Application to hydrogen in α-zirconium, Phys. Rev. B 94 (2016) 241112. doi:10.1103/PhysRevB.94.241112.

[44] G. J. Ackland, Theoretical study of the effect of point defects on the elastic constants of copper, J. Nucl. Mater. 152 (1988) 53–63. doi:10.1016/0022-3115(88)90140-7.

[45] A. F. Bialon, T. Hammerschmidt, R. Drautz, Ab initio study of boron in α-iron: Migration barriers and interaction with point defects, Phys. Rev. B 87 (2013) 104109. doi:10.1103/PhysRevB.87.104109.

[46] M. R. Fellinger, L. G. H. Jr., D. R. Trinkle, Ab initio calculations of the lattice parameter and elastic stiffness coefficients of bcc Fe with solutes, Comp. Mater. Sci. 126 (2017) 503–513. doi:10.1016/j.commatsci.2016.09.040.

[47] E. Clouet, L. Ventelon, F. Willaime, Dislocation core field. II. Screw dislocation in iron, Phys. Rev. B 84 (2011) 224107. doi:10.1103/PhysRevB.84.224107.

[48] C. S. Roberts, Effect of carbon on the volume fractions and lattice parameters of retained austenite and martensite, Trans. AIME 197 (1953) 203–204.

[49] L. Cheng, A. Bottger, T. H. de Keijser, E. J. Mittemeijer, Lattice parameters of iron-carbon and iron-nitrogen martensites and austenites, Scripta Metall. Mater. 24 (1990) 509–514. doi:10.1016/0956-716X(90)90192-J.

[50] A. Nowick, W. Heller, Anelasticity and stress-induced ordering of point defects in crystals, Adv. Phys. 12 (1963) 251–298. doi:10.1080/00018736300101293.

[51] J. C. Swartz, J. W. Shilling, A. J. Schwoeble, Dipolar strains of c and n in alpha-iron, Acta Metall. 16 (1968) 1359–1364. doi:10.1016/0001-6160(68)90156-9.

[52] H. Trinkaus, On determination of the double-force tensor of point defects in cubic crystals by diffuse x-ray scattering, Phys. Stat. Sol. B 51 (1972) 307–319. doi:10.1002/pssb.2220510131.

[53] O. Bender, P. Ehrhart, Self-interstitial atoms, vacancies and their agglomerates in electron-irradiated nickel investigated by diffuse scattering of X-rays, J. Phys. F: Metal. Phys. 13 (1983) 911. doi:10.1088/0305-4608/13/5/006.

[54] T. Michelitsch, A. Wunderlin, On the theory of Huang X-ray scattering caused by point defects in hexagonal crystals, Phys. Stat. Sol. B 198 (1996) 615–620. doi:10.1002/pssb.2221980206.

[55] E. Clouet, S. Garruchet, H. Nguyen, M. Perez, C. S. Becquart, Dislocation interaction with C in α-Fe: A comparison between atomic simulations and elastic theory, Acta Mater. 56 (2008) 3450–3460. doi:10.1016/j.actamat.2008.03.024.

[56] R. G. A. Veiga, M. Perez, C. S. Becquart, E. Clouet, C. Domain, Comparison of atomistic and elasticity approaches for carbon diffusion near line defects in α-iron, Acta Mater. 59 (2011) 6963–6974. doi:10.1016/j.actamat.2011.07.048.

[57] P. H. Dederichs, K. Schroeder, Anisotropic diffusion in stress fields, Phys. Rev. B 17 (1978) 2524. doi:10.1103/PhysRevB.17.2524.

[58] A. H. Cottrell, B. A. Bilby, Dislocation theory of yielding and strain ageing of iron, Proc. Phys. Soc. London Ser. A 62 (1949) 49. doi:10.1088/0370-1298/62/1/308.

[59] C. Woo, Irradiation creep due to elastodiffusion, J. Nucl. Mater. 120 (1984) 55 – 64. doi:10.1016/0022-3115(84)90170-3.

[60] M. J. Aziz, Thermodynamics of diffusion under pressure and stress: Relation to point defect mechanisms, Appl. Phys. Lett. 70 (1997) 2810–2812. doi:10.1063/1.119066.

[61] M. S. Daw, W. Windl, N. N. Carlson, M. Laudon, M. P. Masquelier, Effect of stress on dopant and defect diffusion in Si: A general treatment, Phys. Rev. B 64 (2001) 045205. doi:10.1103/PhysRevB.64.045205.

[62] G. H. Vineyard, Frequency factors and isotope effects in solid state rate processes, J. Phys. Chem. Solids 3 (1957) 121. doi:10.1016/0022-3697(57)90059-8.

[63] R. G. A. Veiga, M. Perez, C. S. Becquart, C. Domain, S. Garruchet, Effect of the stress field of an edge dislocation on carbon diffusion in α-iron: Coupling molec-

ular statics and atomistic kinetic Monte Carlo, Phys. Rev. B 82 (2010) 054103. doi:10.1103/PhysRevB.82.054103.

[64] A. Goyal, S. R. Phillpot, G. Subramanian, D. A. Andersson, C. R. Stanek, B. P. Uberuaga, Impact of homogeneous strain on uranium vacancy diffusion in uranium dioxide, Phys. Rev. B 91 (2015) 094103. doi:10.1103/PhysRevB.91.094103.

[65] R. E. Howard, A. B. Lidiard, Matter transport in solids, Rep. Prog. Phys. 27 (1964) 161–240. doi:10.1088/0034-4885/27/1/305.

[66] A. R. Allnatt, A. B. Lidiard, Atomic Transport in Solids, Cambridge University Press, 1993.

[67] D. R. Trinkle, Diffusivity and derivatives for interstitial solutes: activation energy, volume, and elastodiffusion tensors, Philos. Mag. 96 (2016) 2714–2735. doi:10.1080/14786435.2016.1212175.

[68] R. Agarwal, D. R. Trinkle, Light-element diffusion in Mg using first-principles calculations: Anisotropy and elastodiffusion, Phys. Rev. B 94 (2016) 054106. doi:10.1103/PhysRevB.94.054106.

[69] A. D. Brailsford, R. Bullough, The rate theory of swelling due to void growth in irradiated metals, J. Nucl. Mater. 44 (1972) 121. doi:10.1016/0022-3115(72)90091-8.

[70] H. Rouchette, L. Thuinet, A. Legris, A. Ambard, C. Domain, Influence of shape anisotropy of self-interstitials on dislocation sink efficiencies in Zr: Multiscale modeling, Phys. Rev. B 90 (2014) 014104. doi:10.1103/physrevb.90.014104.

[71] P. T. Heald, The preferential trapping of interstitials at dislocations, Philos. Mag. 31 (1975) 551. doi:10.1080/14786437508226537.

[72] H. Rouchette, L. Thuinet, A. Legris, A. Ambard, C. Domain, Quantitative phase field model for dislocation sink strength calculations, Comp. Mater. Sci. 88 (2014) 50. doi:10.1016/j.commatsci.2014.02.011.

[73] H. L. Heinisch, B. N. Singh, S. I. Golubov, The effects of one-dimensional glide on the reaction kinetics of interstitial clusters, J. Nucl. Mater. 283–287 (2000) 737. doi:10.1016/s0022-3115(00)00258-0.

[74] L. Malerba, C. S. Becquart, C. Domain, Object kinetic Monte Carlo study of sink strengths, J. Nucl. Mater. 360 (2007) 159. doi:10.1016/j.jnucmat.2006.10.002.

[75] K. Schroeder, K. Dettmann, Diffusion reactions in long range potentials, Z. Phys. B 22 (1975) 343. doi:10.1007/bf01312804.

[76] C. H. Woo, The sink strength of a dislocation loop in the effective medium approximation, J. Nucl. Mater. 98 (1981) 279. doi:10.1016/0022-3115(81)90154-9.

[77] B. C. Skinner, C. H. Woo, Shape effect in the drift diffusion of point defects into straight dislocations, Phys. Rev. B 30 (1984) 3084–3097. doi:10.1103/PhysRevB.30.3084.

[78] C. H. Woo, W. S. Liu, M. S. Wuschke, A finite-difference calculation of point defect migration into a dislocation loop, Tech. Rep. AECL-6441, Atomic Energy of Canada Limited (1979).

[79] R. Bullough, D. W. Wells, J. R. Willis, M. H. Wood, The interaction energy between interstitial atoms and dislocations and its relevance to irradiation damage processes, in: M. F. Ashby, R. Bullough, C. S. Hartley, J. P. Hirth (Eds.), Dislocation Modelling of Physical Systems, Pergamon, 1981, p. 116.

[80] V. I. Dubinko, A. S. Abyzov, A. A. Turkin, Numerical evaluation of the dislocation loop bias, J. Nucl. Mater. 336 (2005) 11. doi:j.jnucmat.2004.07.034.

[81] T. Jourdan, Influence of dislocation and dislocation loop biases on microstructures simulated by rate equation cluster dynamics, J. Nucl. Mater. 467 (2015) 286. doi:j.jnucmat.2015.09.046.

[82] A. B. Sivak, V. M. Chernov, V. A. Romanov, P. A. Sivak, Kinetic monte-carlo simulation of self-point defect diffusion in dislocation elastic fields in bcc iron and vanadium, J. Nucl. Mater. 417 (2011) 1067–1070. doi:10.1016/j.jnucmat.2010.12.176.

[83] A. Vattré, T. Jourdan, H. Ding, M.-C. Marinica, M. J. Demkowicz, Non-random walk diffusion enhances the sink strength of semicoherent interfaces, Nat. Commun. 7 (2016) 10424. doi:10.1038/ncomms10424.

[84] D. T. Gillespie, A general method for numerically simulating the stochastic time evolution of coupled chemical reactions, J. Comput. Phys. 22 (1976) 403. doi:10.1016/0021-9991(76)90041-3.

[85] A. B. Bortz, M. H. Kalos, J. L. Lebowitz, A new algorithm for Monte-Carlo simulation of ising spin systems, J. Comput. Phys. 17 (1975) 10. doi:10.1016/0021-9991(75)90060-1.

[86] A. Vattré, M. Demkowicz, Determining the Burgers vectors and elastic strain energies of interface dislocation arrays using anisotropic elasticity theory, Acta Mater. 61 (2013) 5172–5187. doi:10.1016/j.actamat.2013.05.006.

[87] A. J. Vattré, M. J. Demkowicz, Partitioning of elastic distortions at a semicoherent heterophase interface between anisotropic crystals, Acta Mater. 82 (2015) 234. doi:10.1016/j.actamat.2014.09.014.

[88] D. Carpentier, T. Jourdan, Y. Le Bouar, M.-C. Marinica, Effect of saddle point anisotropy of point defects on their absorption by dislocations and cavities, Acta Mater. 136 (2017) 323. doi:10.1016/j.actamat.2017.07.013.

[89] V. A. Borodin, A. I. Ryazanov, C. Abromeit, Void bias factors due to the anisotropy of the point defect diffusion, J. Nucl. Mater. 207 (1993) 242. doi:10.1016/0022-3115(93)90266-2.

[90] V. A. Borodin, A. I. Ryazanov, The effect of diffusion anisotropy on dislocation bias and irradiation creep in cubic lattice materials, J. Nucl. Mater. 210 (1994) 258. doi:10.1016/0022-3115(94)90180-5.

[91] J. E. Sinclair, P. C. Gehlen, R. G. Hoagland, J. P. Hirth, Flexible boundary conditions and nonlinear geometric effects in atomic dislocation modeling, J. Appl. Phys. 49 (1978) 3890–3897. doi:10.1063/1.325395.

[92] S. Rao, C. Hernandez, J. P. Simmons, T. A. Parthasarathy, C. Woodward, Green's function boundary conditions in two-dimensional and three-dimensional atomistic simulations of dislocations, Philos. Mag. A 77 (1998) 231–256. doi:10.1080/01418619808214240.

[93] Y. Liu, G. Lu, Z. Chen, N. Kioussis, An improved QM/MM approach for metals, Modelling Simul. Mater. Sci. Eng. 15 (2007) 275–284. doi:10.1088/0965-0393/15/3/006.

[94] X. Zhang, G. Lu, W. A. Curtin, Multiscale quantum/atomistic coupling using constrained density functional theory, Phys. Rev. B 87 (2013) 054113. doi:10.1103/PhysRevB.87.054113.

[95] L. Huber, B. Grabowski, M. Militzer, J. Neugebauer, J. Rottler, A QM/MM approach for low-symmetry defects in metals, Comp. Mater. Sci. 118 (2016) 259–268. doi:10.1016/j.commatsci.2016.03.028.

[96] M. Leslie, N. J. Gillan, The energy and elastic dipole tensor of defects in ionic crystals calculated by the supercell method, J. Phys. C Solid State 18 (1985) 973–982. doi:10.1088/0022-3719/18/5/005.

[97] G. Makov, M. C. Payne, Periodic boundary conditions in *ab initio* calculations, Phys. Rev. B 51 (1995) 4014–4022. doi:10.1103/PhysRevB.51.4014.

[98] S. E. Taylor, F. Bruneval, Understanding and correcting the spurious interactions in charged supercells, Phys. Rev. B 84 (2011) 075155. doi:10.1103/PhysRevB.84.075155.

[99] C. Varvenne, F. Bruneval, M.-C. Marinica, E. Clouet, Point defect modeling in materials: Coupling *ab initio* and elasticity approaches, Phys. Rev. B 88 (2013) 134102. doi:10.1103/PhysRevB.88.134102.

[100] W. Cai, V. V. Bulatov, J. Chang, J. Li, S. Yip, Periodic image effects in dislocation modelling, Philos. Mag. 83 (2003) 539–567. doi:10.1080/0141861021000051109.

[101] M.-C. Marinica, F. Willaime, J.-P. Crocombette, Irradiation-induced formation of nanocrystallites with $c15$ laves phase structure in bcc iron, Phys. Rev. Lett. 108 (2012) 025501. doi:10.1103/PhysRevLett.108.025501.

[102] R. C. Pasianot, Self-interstitials structure in the hcp metals: A further perspective from first-principles calculations, J. Nucl. Mater. 481 (2016) 147–152. doi:10.1016/j.jnucmat.2016.09.021.

[103] M. Souissi, Y. Chen, M. H. Sluiter, H. Numakura, Ab initio characterization of B, C, N, and O in bcc iron: Solution and migration energies and elastic strain fields, Comp. Mater. Sci. 124 (2016) 249–258. doi:10.1016/j.commatsci.2016.07.037.